CHAPTER II

Measurement of Spontaneous Polarisation

2.1 Introduction

The magnitude of the spontaneous polarisation P_s is obviously of fundamental importance in determining tlie operating characteristics of a ferroelectric liquid crystal **(FLC)** device.[1–3] To synthesise **FLC** materials with large P_s, and hence lower operating voltages, it is essential to know the relationship between magnitude of P_s and the molecular structure.[4,5] The symmetry considerations which predict[1] the existence of ferroelectricity in liquid crystals do not give any information concerning the magnitude of P_s. Despite a number of studies[6–8] in this direction, the delicate interplay between the molecular structure and tlie P_s values is not well understood. However, these studies have helped in framing some empirical rules. The major factors which have been found to control tlie magnitude of P_s are:

1. tlie size of tlie lateral dipole moment at the cliiral centre,[9]
2. the degree to which the rotations of the molecules especially the chiral centre are hindered,[10]

3. tlie degree of tlie coupling between tlie dipole at tlie chiral centre with any other dipoles in tlie molecule,[11]

4. tlie distance between the chiral centre and the central rigid core,[12]

5. the alkyl chain length.[13–15]

However, not many systematic experimental studies had been done to check the validity of some of these conclusions.

This chapter describes systematic measurements of P_s on a number of compounds belonging to four structurally similar honiologues series. The studies bring out the influence of several factors like (a) the length of the alkyl chains, (b) the number of chiral centres, (c) spacer groups between the chiral group and the core, etc., on the magnitude of P_s.

The chapter begins with a detailed description of tlie experimental set-up including the apparatus used to measure P_s, the techniques employed for alignment of the sample, the temperature control and the hardware/software for programmed acquisition and analysis of the data, followed by tlie results obtainetl for tlie four series of compounds. Finally, some of the features observed are discussed in terms of a microscopic[16,17] theory.

2.2 Materials

As tlie aim was to study the effect of subtle changes in the molecular structure on the magnitude of P_s, care was taken in selecting tlie materials. The compounds chosen belong to four different homologues series and were synthesised in our laboratory.[18] Tlie compounds are basically derivatives of *trans*-p-n-alkoxy cinnarnate. In all the four series, for convenience referred to as series A,B,C and D, tlie homologues with n

= 7 to 12 (where n denotes tlie number of carbon atoms in tlie chain) exhibit SmC* phase over a large temperature range (more than 10°C). The structural formulae, phase transition temperatures along with tlie heats of transition are given in tables 2.1 to 2.4. In compounds of both series D arid B there are two asymmetric carbon atoms, the difference being that in series D the chiral group is attached directly to the core, but is separated by a CH_2 spacer in series B (for all practical purposes the COO group at one end of tlie core is considered to be a part of the core).[19] This feature is retained between series C arid **A** but in both of them the number of chiral centres is reduced to one. Thus the studies would bring out the different factors influencing the magnitude of P_s, for example, effect of the spacer group when two chiral atoms are present (series D and B) and when one chiral atom is present (series C and A), effect of an additional chiral atom when the core is close to it (series D and C) or with a spacer between (series B and A), arid the effect of chain length.

Another significant feature of these series of compounds is the temperature range of the smectic A phase - which has been observed[20–22] to determine the nature of tlie SmA-SmC* transition - decreases as the chain length increases (see Figs. 2.1a-2.1d). Not many reports of such behaviour exists in the literature. Arid probably this is tlie first study where this reverse trend has been mentioned with its importance.

2.3 Experimental

2.3.1 The sample cell

Electrically, tlie sample cell can he considered as a parallel plate capacitor. It is made up of two thin (thickness ~0.7 mm), flat and transparent glass plates (Balzers, Switzerland) made conducting by Indium tin oxide (ITO) coating. The glass plates have tlie required electrode pattern (see Fig.2.2) etchecl on them by using dilute

Table 2.1

Transition temperature (°C) and heats of transition (kcals/mole) of A,-series

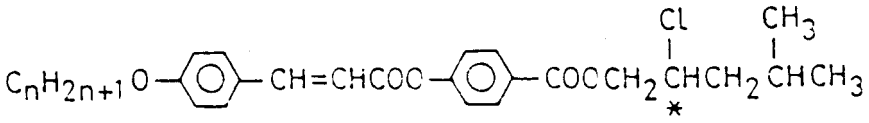

n	K	C*	A	Ch	I
6	. 51.5 9.1	(. 41.5) 0.05	. 78.0 0.35	. 80.5 0.2	.
7	. 57.5 7.9	(. 50.0) 0.01	. 74.5 0.25	. 77.0 0.22	.
8	. 50.0 5.8	. 56.5 0.08	. 79.5 0.21	. 80.2 0.16	.
9	. 62.0 10.0	(. 60.5) 0.1	. 78.0 0.2	. 79.0 0.2	.
10	. 44.0 7.7	. 63.5 0.09	. 81.1 0.9	–	.
11	. 55 .5 9.1	. 64.5 0.06	. 80.5 0.9	–	.
12	. 52.0 8.1	. 65.5 0.01	. 81.0 1.0	–	.

K-= crystal, C* = chiral smectic C,
A = smectic **A,** Ch = chiral nematic and
I = isotropic phase.
The temperature in parentheses indicate a monotropic transition
*These compounds exhibit a blue phase.

Table 2.2

Transition temperature (°C) and heats of transition (kcals/mole) of B_n-series

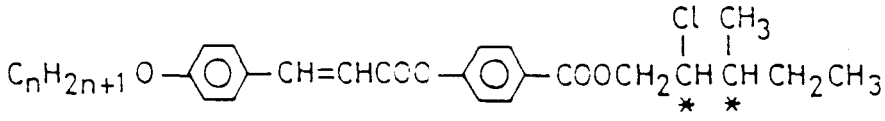

n	K	C*	A	Ch	I
6	71.0 5.2	–	83.5 0.4	84.5 0.1	
7	64.5 8.1	(. 52.5) 0.05	80.5 0.2	82.5 0.14	
8	57.0 7.3	59.0 0.04	84.5 0.3	85.0 0.2	
9	52.0 6.8	64.0 0.05	85.0 0.8	–	
10	42.5 7.2	66.5 0.05	87.0 0.09	–	
11	62.5 9.2	68.5 0.04	88.5 0.97	–	
12	53.5 10.5	69.5 0.05	88.5 1.4	–	

Table 2.3

Transition temperature (°C) and heats of transition (kcals/mole) of C_n-series

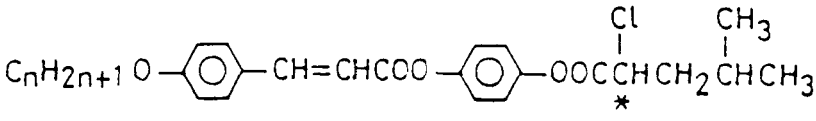

n	K	C*	A	I
6	. 81.5	(. 56.0)	. 93.5	.
	6.01	0.04	0.96	
7	. 55.0	. 67.0	. 90.5	.
	8.16	0.05	0.81	
8	. 62.0	. 73.0	. 92.5	.
	5.80	0.05	0.97	
9	. 73.0	. 75.5	. 90.5	.
	6.13	0.06	1.0	
10	. 69.0	. 78.0	. 92.5	.
	5.59	0.05	0.92	
11	. 54.0	. 79.0	. 92.0	.
	6.43	0.04	1.04	
12	. 62.0	. 80.0	. 92.5	.
	7.5	0.05	1.0	

Table 2.4

Transition temperature (°C) and heats of transition (kcals/mole) of D_n-series

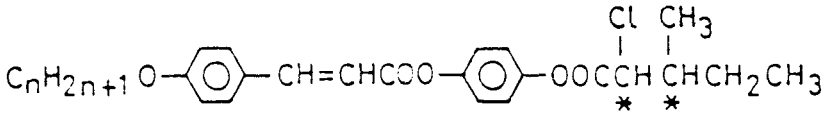

n	K	C*	A	Ch	I
6	. 81.0 6.0	. 56.5 0.03	. 90.5 0.13	. 98.5 0.14	.
7	. 61.5 8.7	. 68.5 0.06	. 88.0 0.12	. 95.0 0.21	.
8	. 61.0 4.5	. 73.0 0.05	. 93.0 0.10	. 96.5 0.18	.
9	. 69.0 7.3	. 78.0 0.06	. 95.0 0.05	. 97.0 0.23	.
10	. 56.0 8.0	. 80.0 0.04	. 98.5 0.07	. 99.0 0.21	.
11	. 50.0 5.43	. 83.5 0.06	. 99.5 0.89	–	.
12	. 56.5 10.8	. 84.5 0.05	. 100.0 1.0	–	.

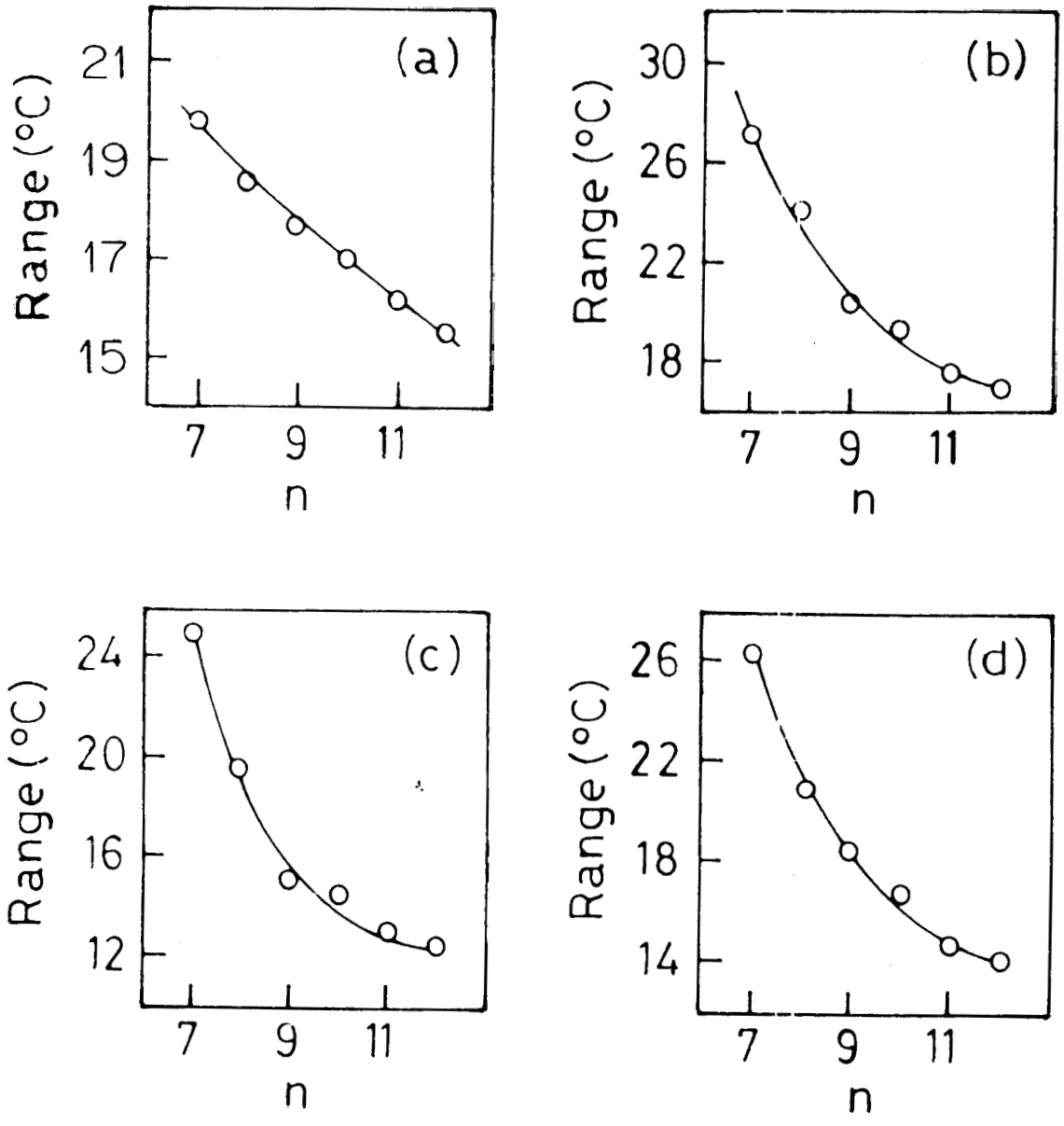

Fig.2.1. Range of the smectic A phase as a function of alkyl chain length for (a) series D, (b) series B, (c) series C and (d) series A

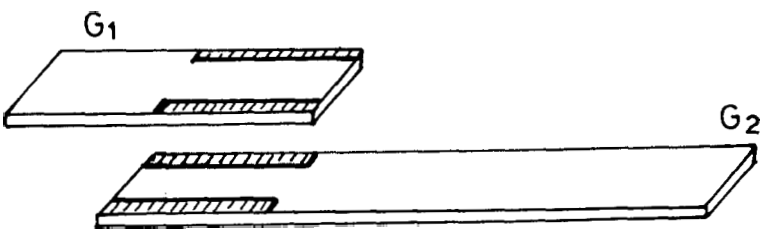

G_1 , G_2 - ITO coated glass plates

Hatched portion - Etched part of the glass plates

Fig.2.2. Schematic diagram of the sample cell.

hydrochloric acid and zinc dust. The two plates, with mylar spacers to define the thickness of the sample, were glued together by a non-conducting and 11011-reactive epoxy (Rhodorsil Silicones CAF4) and cured at suitable temperature in an oven. (This epoxy was found to be effective even up to 200°C.) While preparing the sample cell, care was taken to see that neither the mylar spacer nor the epoxy enter the active area. This ensures the proper determination of the active area of the sample. After preparing tlie cell its thickness was measured to a high precision ($<0.1\ \mu m$) by optical interference technique.[23] Only those cells which had uniform thickness throughout tlie active area were chosen for the experiments. For accurate P_s measurements an accurate value of the active area of tlic cell is necessary. For this purpose the capacitance technique was employed. The capacitance of the empty cell C_o, was accurately measured by an impedance analyses (HP 4192 A). The area 'A' of tlie cell was calculated knowing tlie value of C_o, the thickness d obtained by the interference method[23] and using tlie relation $A = \frac{C_o d}{\epsilon_o}$, where ϵ_o is the permittivity of the free space. Using this procedure the accuracy in tlic determination of the area is reckoned to be better than ±2% of the actual value.

2.3.2 Sample cell holder and heater assembly

Since tlie transitions studied were at temperatures higher than the ambient temperature, an efficient but convenient cell holder and heater assembly was necessary. While constructing such an assembly certain factors had to be borne in mind.

1. tlie temperature over the entire area of tlie sample sliould be very uniform,
2. it sliould be possible to raise or lower the sample temperature over a. wide range (room temperature to 150°C),
3. the sample temperature sliould be measured with high precision,

4. tlie heater assembly should be able to hold the sample temperature over periods of $\sim$ 10 minutes with minimal drift,

5. it should be conveniently possible to apply *a* magnetic field for sample alignment.

Keeping these facts in mind a cell holder heating assembly was designed and constructed. The schematic diagram of the heater is shown in Fig. **2.3.** The heater is made up of a rectangular copper block. At the centre of this block a slot was made along its length for tlie sample cell. Kapton based thermofoil heater (Minco) strips were wrapped around the copper block by taking care to see that the thermal power would be uniformly spread out. This ensures a uniform heating of the block and hence that of the sample cell placed inside the block. The copper block was covered on all sides by thick PTFE (Teflon) sheets which provide very good thermal insulation. A small circular hole (diameter $\sim$ **3** mm) running through tlie body of the heater served as an optical window to check the alignment of tlie sample as well as to monitor the transition temperature. Both tlie entrance and exit sides of tlie window are covered by thin mylar strips to avoid any air currents affecting tlie sample temperature. A screw threaded into the body and positioned near the opening made to introduce the glass cell, holds the cell flush with the surface of the copper block and ensures uniform heating of the cell. The tip of this screw is made of an insulating material to minimise the heat losses. The foil heaters provided an effective heating capacity of about 50 watts. The power input to the foils was controlled using a programmable high stability DC power supply (Ilewlett I'ackard, Model 6038A).

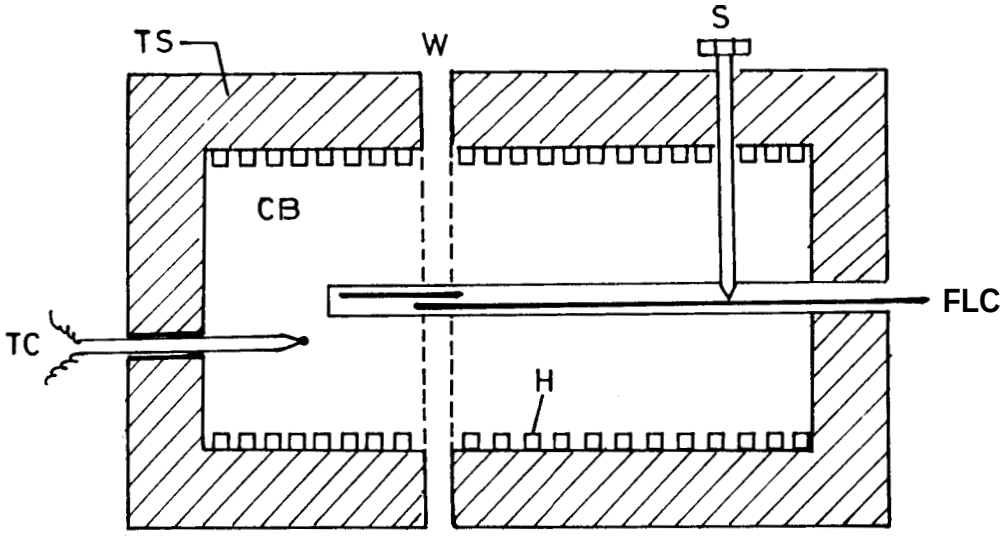

Sectional View

CB : Copper block

TS: Teflon shield

FLC : Sample cell

TC : Thermocouple

S : Screw to fix the Sample cell

W : Window for optical observation

H : Thermofoil heater

Fig.2.3. Cross sectional view of the sample oven assembly.

2.3.3 Temperature control and measurement

For tlie measurement arid control of tlic sample temperature an embedded chromel-constantan thermocouple was used. There are two reasons for the selection of this thermocouple - (1) both chromel and constantan are non-magnetic materials arid so the temperature calibration is valid in the presence of a magnetic field also, (2) The thermo e.m.f. for this particular thermocouple is high ($\approx 60\mu V/^{\circ}C$) and therefore the temperature can be measured with a very high degree of accuracy. The thermocouple was located at tlie centre of tlie copper block and was fixed in position with a high temperature adhesive. The thermo e.m.f. of the thermocouple was measured using a high resolution, low drift digital nanovoltmeter (Keithley 181) which was interfaced to a microcomputer through the IEEE 488 bus.

The large thermal capacity of the heater combined with better insulation enabled the temperature to be maintained to a constancy of better than $\pm$ 3 mK over short periods ($\sim$10 minutes).

2.3.4 Temperature calibration of the cell

Calibration of the thermocouple was carried out using several liquid crystalline materials that were of high chemical purity and exhibited sharp phase transitions. The compounds used along with their transition temperatures, as measured using a polarizing microscope in conjunction with a commercially available programmable hot stage (Mettler FP82), tlie thermocouple output are listed in tlie table 2.5. A plot of the Mettler transition temperatures vs. the corresponding thermo emf (mV) is shown in Fig.2.4. It is known that the temperature vs. thermo ernf curves can be described by polynomials. Figure 2.4 also show tlie fit of the data to a polynomial of the type $T = A, + A_1X + A_2X^2 + A_3X^3 + A_4X^4$ (where T is tlie temperature in

Table 2.5

Compounds used in the temperature calibration of the sample oven and their nematic-isotropic transition temperature

Compound	Mettler Temp (°C)	Thermocouple emf (mV)
5CB	33.44	2.003
7CB	40.5	2.4688
9CB	49.95	3.0784
408	77.7	4.873
7OPDOB	88.32	5.582
CBOOA	107.8	6.918
PAA	135.75	8.8667

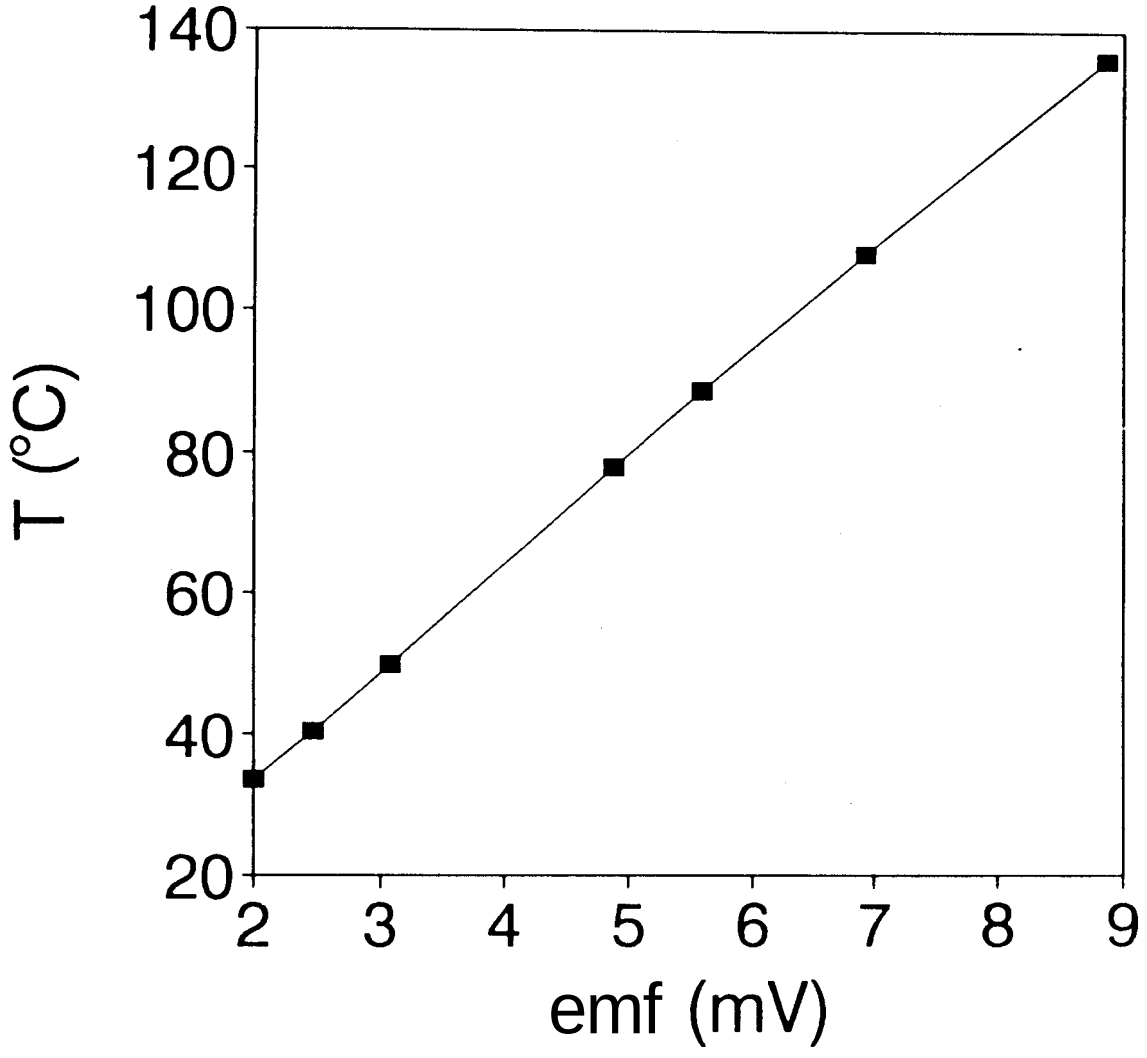

Fig.2.4. Temperature calibration curve of the sample oven using the substances listed in Table 2.5; ■ Squares represent experimental points and the line fit to a polynomial.

^oC arid X tlie thermo emf in (mV) using a least square fit programme. The values obtained for the constants are listed below.

1. A, = 6.7084
2. $A_1 = 10.988$
3. $A_2 = 1.5856$
4. $A_3 = -0.2248$
5. $A_4 = 1.03E\text{-}2$

2.3.5 The sample alignment

A convenient way of measuring P_s of a FLC is to have the sample aligned in the homogeneous (planar) bookshelf geometry.[2] Here the smectic layers will be perpendicular to the glass plates (electrodes) and thus tlie field is applied parallel to the smectic layers and perpendicular to the director n (see Fig. 2.5). A proven method[24] for realising well oriented samples is by surface treatement of the substrate. For this purpose, tlie ITO coated plates were treated with polyimide solution and rubbed unidirectionally, after wliicli the cell was assembled as described earlier. The sample was filled into the cell in the isotropic state by capillary action. Care was taken to see that tlie sample is filled uniformly witliout any air bubbles. As a last step towards obtaining good alignment,, the sample was heated to a temperature slightly above the isotropic point arid cooled slowly, across the Iso-SmA or Iso-Ch-SmA, at a rate of $2 \sim 3^oC$/hour. This procedure generally resulted in a monodomain smectic A phase. However, in a few cases application of a magnetic field, while cooling from the isotropic phase, was also necessary. The direction of the magnetic field

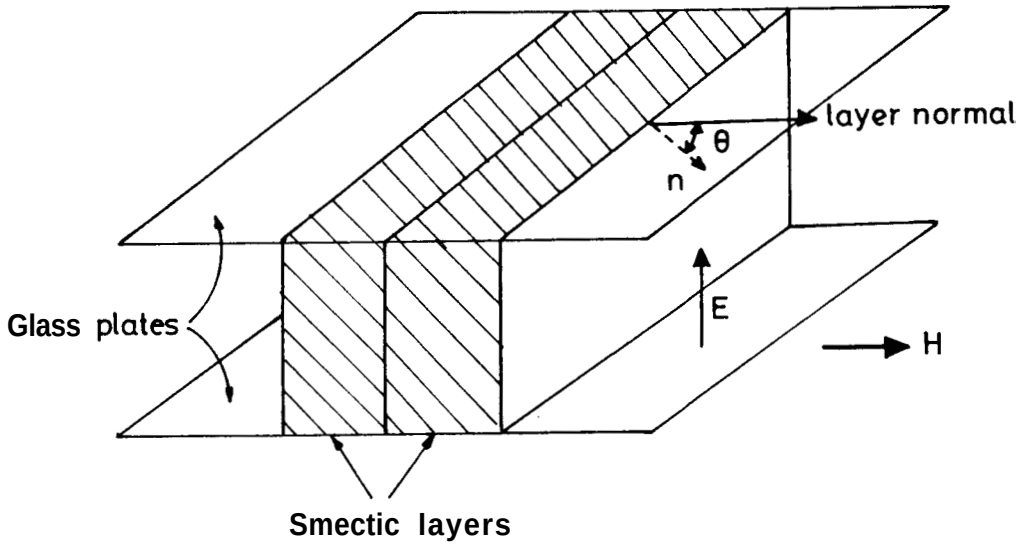

Fig.2.5. Schematic diagram of the alignment of molecules in the "book shelf geometry".

(maximum strength 2.4 T obtained by a Bruker BE25 electromagnet) was parallel to tlie plane of the glass plates and the rubbing direction (see Fig. 2.5).

2.3.6 Measurement of spontaneous polarisation (P_s)

Several rncthotls employed for tlie measurement of P_s in solid ferroelectrics, have been used in tlie case of FLCs also.[25–27] In addition, a few techniques liave been developed specifically for liquid crystals.[28–31] Among these a successful and very versatile method is tlie Diamant bridge[32] method. We liave aclopted tliis modified form of the Sawyer-Tower[33] bridge, the principle of wliicli is described briefly. In the Sawyer-Tower circuit (Fig. 2.6a) a low frequency sine-wave a.c. field of sufficiently high amplitude is applied to tlie ferroelectric sample. A plot of the input versus output signals produces a hysteresis loop characteristic[34] of a ferroelectric material. Tlie P_s is extracted by extrapolating tlie linear part of the loop to E = 0 (see Fig. 2.6b). Tlie main drawback of tliis simple method is that if the output consists even a small part of ionic and linear capacitive contributions then tlie loop gets distorted (Fig.2.6c) making it difficult to measure P_s accurately. A modified version of tliis, proposed by Diamant et *al.*,[32] overcomes this problem. In tliis method, also usually referred to as tlie hysteresis loop method, two parallel Sawyer-Tower circuits are used, one containing tlie sample and tlie other a resistor capacitor combination, both of wliicli can be independently varied. The latter enables compensation of ionic and linear capacitive portions of tlie output signal. This is achieved by feeding the output from the sample and tlie compensating Sawyer-Tower circuit to a difference amplifier.

The Diamant bridge circuit along with a schematic diagram of the data acquisition system used is shown in the Fig.2.7a. Tlie bridge is balanced by the

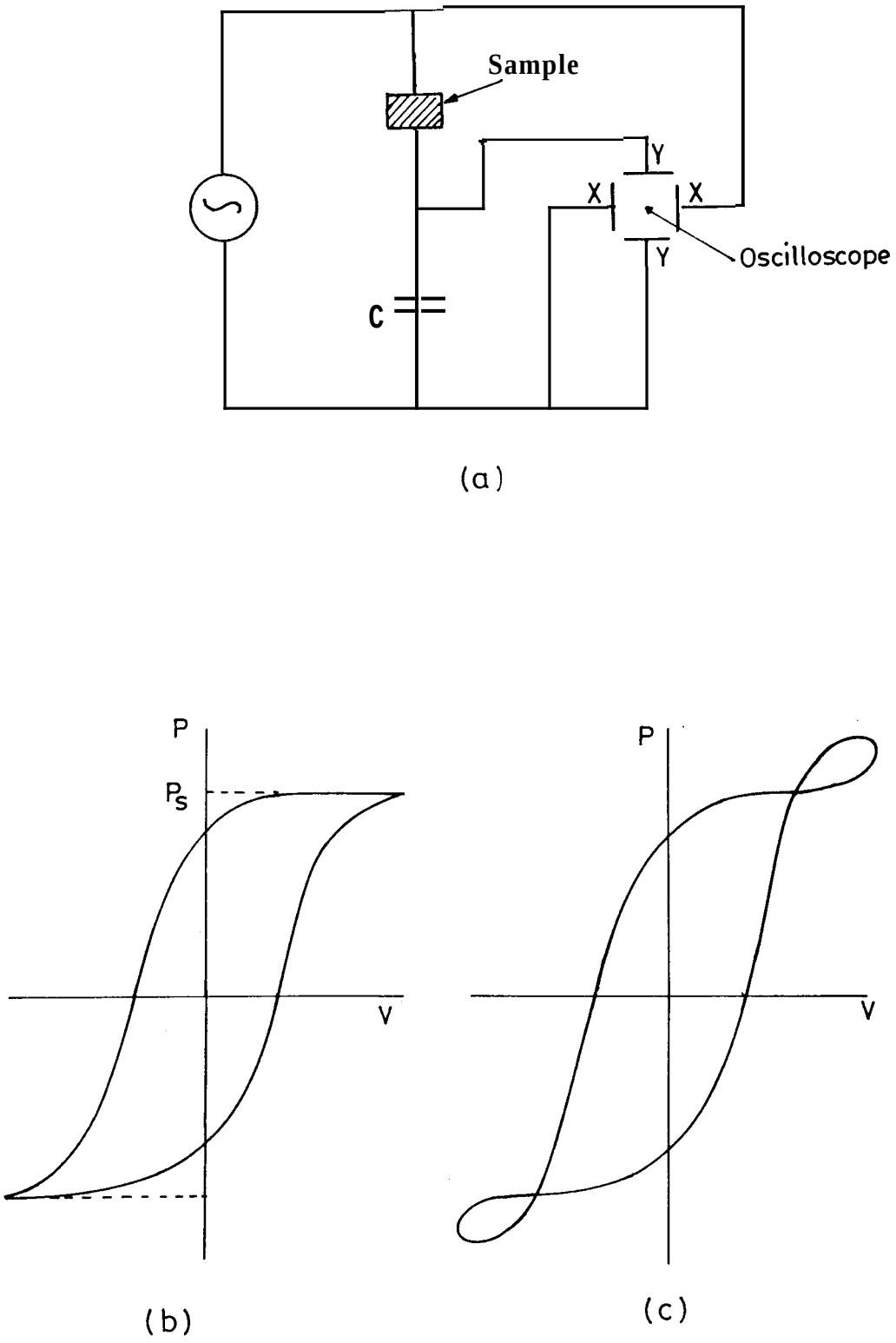

Fig.2.6. (a) Circuit diagram of the Sawyer Tower bridge. Hysteresis loop from: (b) an ideal sample, *(c)* sample having finite ionic contribution.

compensating capacitors and resistors C_C & R_C. A six decade variable resistance (smallest step 0.1 kΩ) box (R_C) was constructed for this purpose. While the capacitor was a commercially available variable five decade capacitor (HP 4440B) made of silvered mica sheets (smallest step 2 pf). Two fixed value capacitors (0.1 μF) form the other two arms of tlie bridge. A function generator (EJP 8116) delivers the sine waves whose amplitude was amplified by a high voltage high fidelity amplifier (Kepco BOP 1000M) and thus the required voltage was applied to the sample. By tuning R_C and C_C values the conductivity and capacitance distortions could be completely corrected. The outputs from the *sample arm* and the *compensating arm* of the bridge were fed to a programmable gain difference amplifier (Analog Devices, AD524) to produce a perfect hysteresis loop (see Fig. 2.7b). The applied and tlie amplifier output signals are then digitised using a digitiser-cum-data acquisition system (HP7090A). This is a 3 channel high resolution (12 bit) and low drift, wide range input (0.1 mV to 100 V) digitiser having a maximum sampling rate of **33,000** samples/sec for each channel and an onboard memory 21 kbytes, enough to hold 3000 data-points. The data thus collected was transferred to an online computer (HP86B) for storage. The data acquisition system and the temperature measuring nanovoltmeter were interfaced to tlie computer through HPIB (IEEE 488) Bus (see Fig.2.7a). By measuring the amplitude V_p of the output wave, P_s can he calculated using tlie relation

$$P_s = \frac{CV_P}{A} \tag{2.1}$$

where C (C_f in tlie Fig. 2.7a) is tlie value of tlie standard capacitor and A tlie active area of the sample cell. Almost full automation of data acquisition arid temperature monitoring enabled collection of data at very close intervals of temperature.

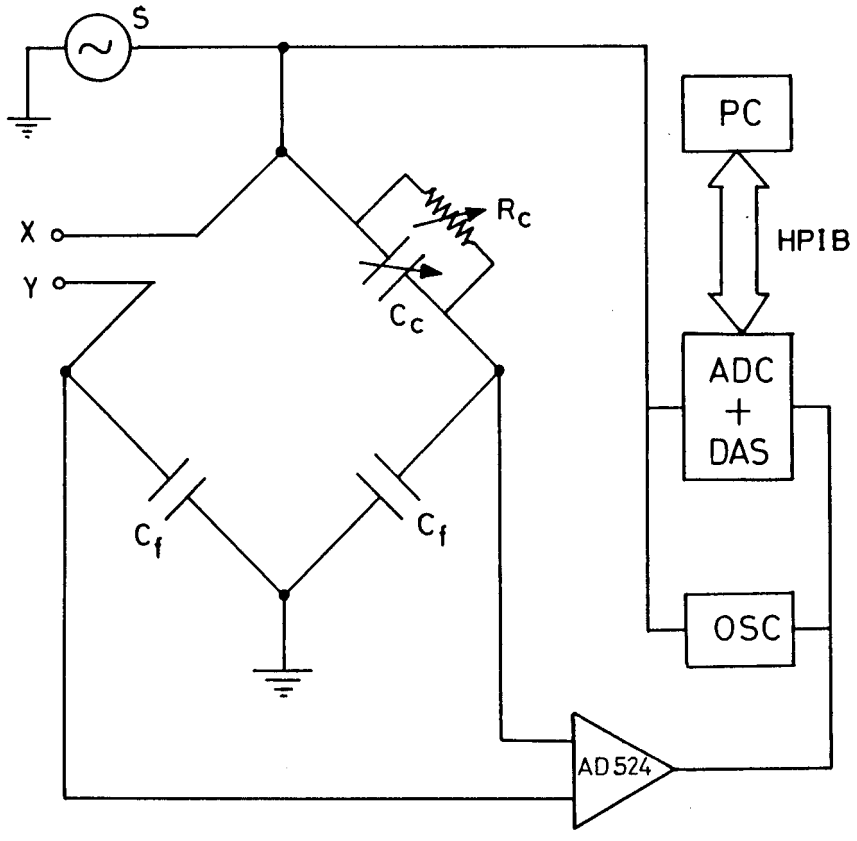

Fig.2.7. (a) Experimental set-up on Diamant bridge technique. S: Signal source; X,Y : Sample leads; R,, C_c : Compensating resistor, Capacitor combination; C_f : Fixed capacitor; OSC : Dual channel storage oscilloscope; ADC + DAS : Analog-Digital Converter and Data Acquisition System; PC : Personal Computer. AD524 is a programmable gain instrumentation operational amplifier.

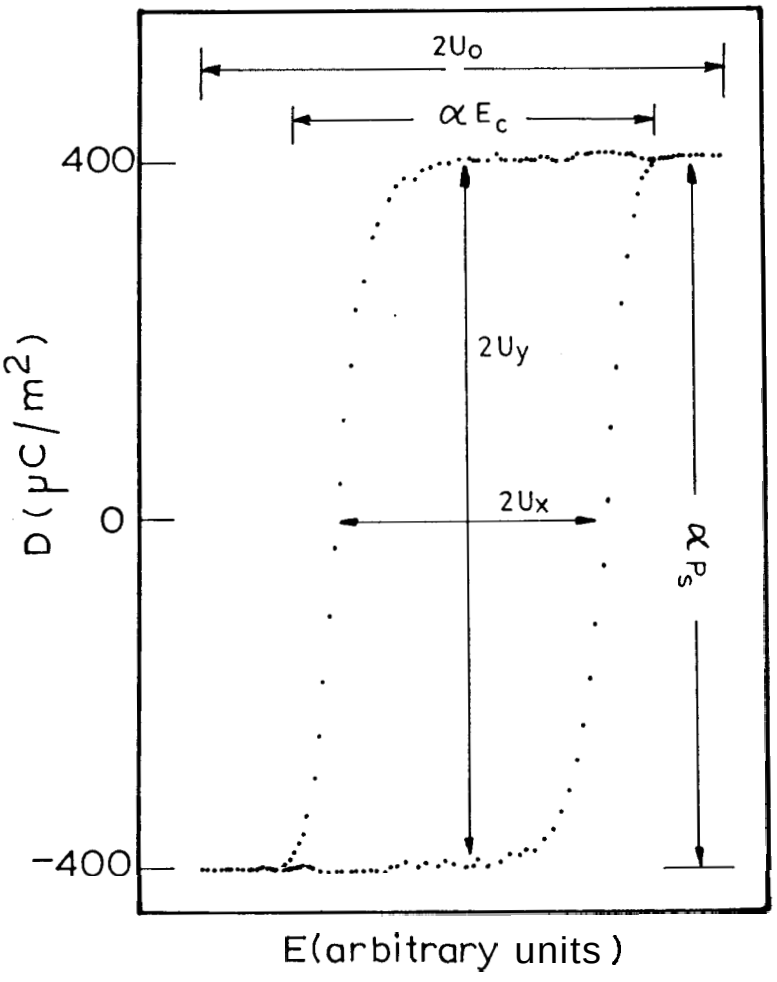

(b) A typical hysteresis loop.

2.3.7 Calibration of the Diamant bridge

The set up was checked electrically as well as by measuring P_s as a function of temperature for two ferroelectric liquid crystalline materials (MCP7OB and CE8) for which such results have already been reported, by Bahr and Heppke[13] for MCP7OB and by Spruce and Pringle[35] for CE8. The data obtained using our set up agrees to within 5% of the values reported for MCP7OB and within 10% for CE8 over the entire temperature range in both cases, as seen from Figs. 2.8a and 2.8b.

While conducting the measurements of P_s we have always cooled the sample $\sim 10°C$ below the A-C* transition temperature and the P_s measurements were done on the heating rnode. Throughout the measurement, the shape of tlie hysteresis loop was monitored using a dual channel storage oscilloscope (Philips PM2203) and the bridge was kept in a balanced condition by adjusting R_C and C_C. The rate of heating was $\sim 6°C$/hour away from T_c and $\sim 1°C$/hour close to T_c. The sample alignment was constantly checked by a polarising microscope.

2.3.8 Measurement of tilt angle

As already pointed out in chapter I, for FLCs P_s is the secondary order parameter arid tlie tilt angle is the primary order parameter.[9] To compare the data with the predictions of the existing theoretical models it would be necessary to know the temperature variation of tilt angle also. For this we measured the tilt angle by the X-ray diffraction method. By measuring the smectic layer spacing d_A in SmA phase and d_{C^*} in SmC* phase the tilt angle is evaluated using the relation $\theta = \cos^{-1}(\frac{d_{C^*}}{d_A})$. Here d_A is the layer spacing value in the SmA phase as measured just before the transition. For the layer spacing measurement in SmA and SmC* phases an existing experimental set up[36] was used, a schematic diagram of which is given in Iig.2.9.

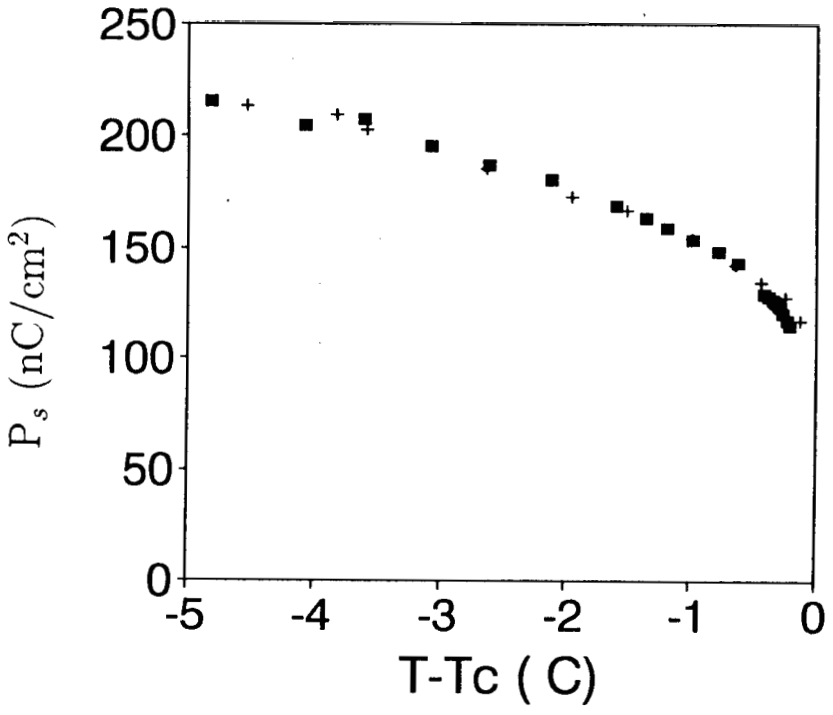

Fig.2.8(a). Comparison of P_s values obtained for MCP7OB from our set-up (□) with those (+) reported by Bahr and Heppke[13].

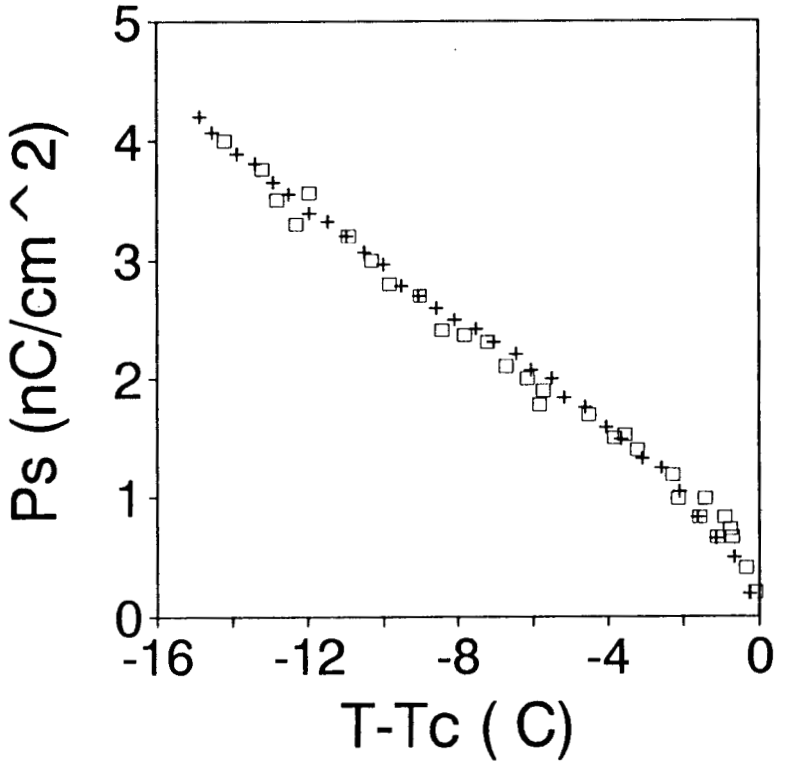

Fig.2.8(b). Comparison of P_s value obtained for CE8 from our set-up (O)with those by Spruce and Pringle.[35]

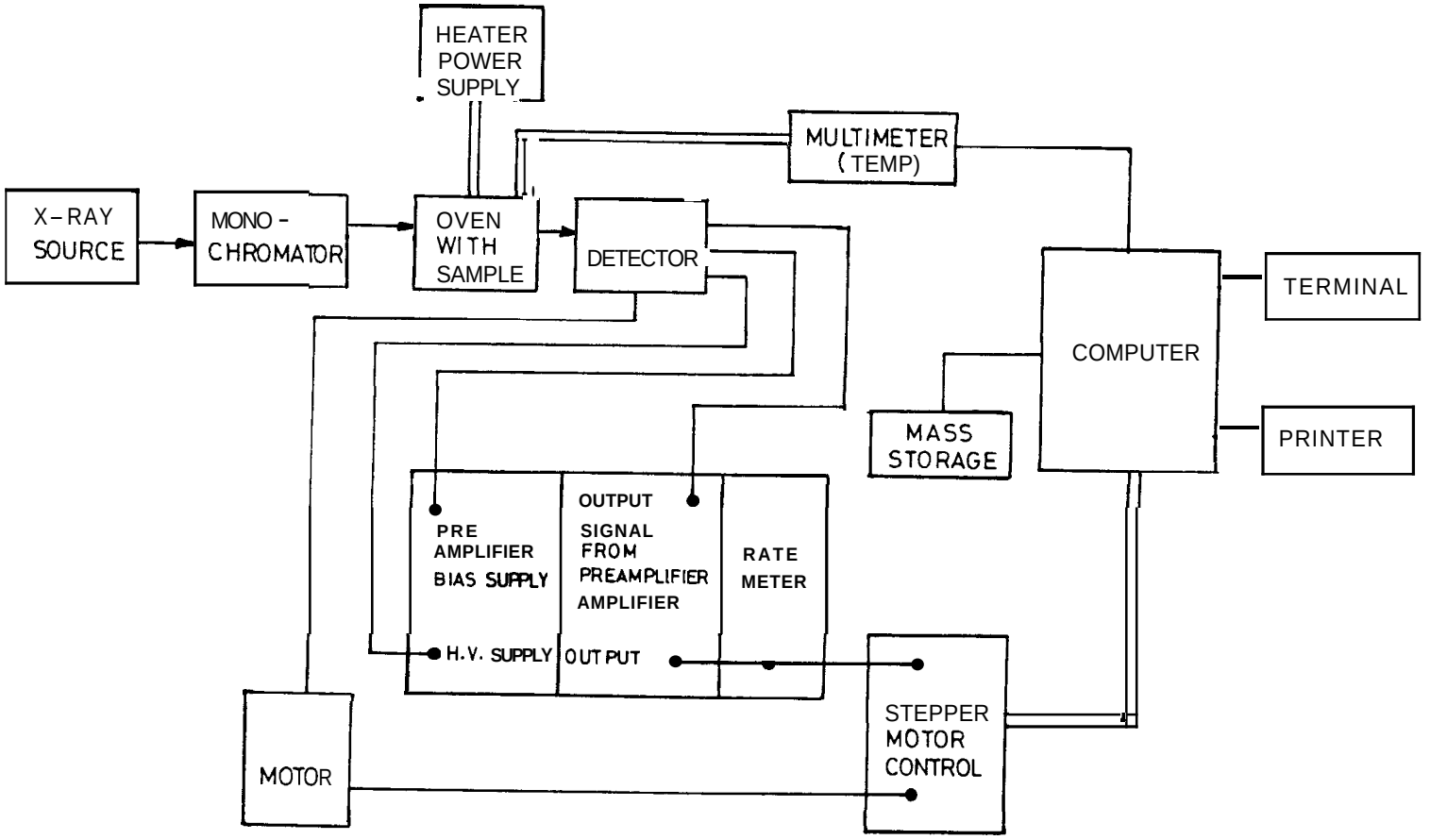

Fig.2.9. Block diagram showing the experimental set-up used for Xray diffraction studies.

The sample was taken in a Lindemann capillary (0.7 mm diameter) both tlie ends of which are sealed. A copper capillary holder was placed inside a temperature coritrolled oven. An aligned SmA phase was obtained by cooling the sample at a slow rate of 3°K/hour from the isotropic phase in the presence of a 2.4 T magnetic field. The aligned sample was then transferred along with the oven to the goniometer head of the diffractometer. Measurements were done using a computer controlled Guinier diffractometer (Huber 644). Copper $K\alpha_1$ and $K\alpha_2$ lines were separated and only $K\alpha_1$ was used for the experiment. During any measurement tlie temperature was kept constant to $\pm 10mK$.

2.4 Results

2.4.1 Series D: Compounds with two chiral centres and without spacer group

Fig.2.10 shows the thermal variation of P_s for the six homologues of this series (n=7 to 12). As expected, for all the compounds P_s is found to decrease with increasing temperature and goes to zero continuously at T_c (T_c is the SmA-SmC* transition temperature). A notable feature is that as the chain length increases, there is a substantial decrease in tlie magnitude of P_s. In addition, the rate at which P_s decreases with temperature, close to T_c, decreases as the chain length is increased. Fig. 2.11 shows a plot of P_s at $T - T_c$ = -10°C versus chain length. It is seen that for the 7th homologue P_s is about 1500 $\mu C/m^2$ whereas for the 12th homologue it, reduces to about 750 $\mu C/m^2$.

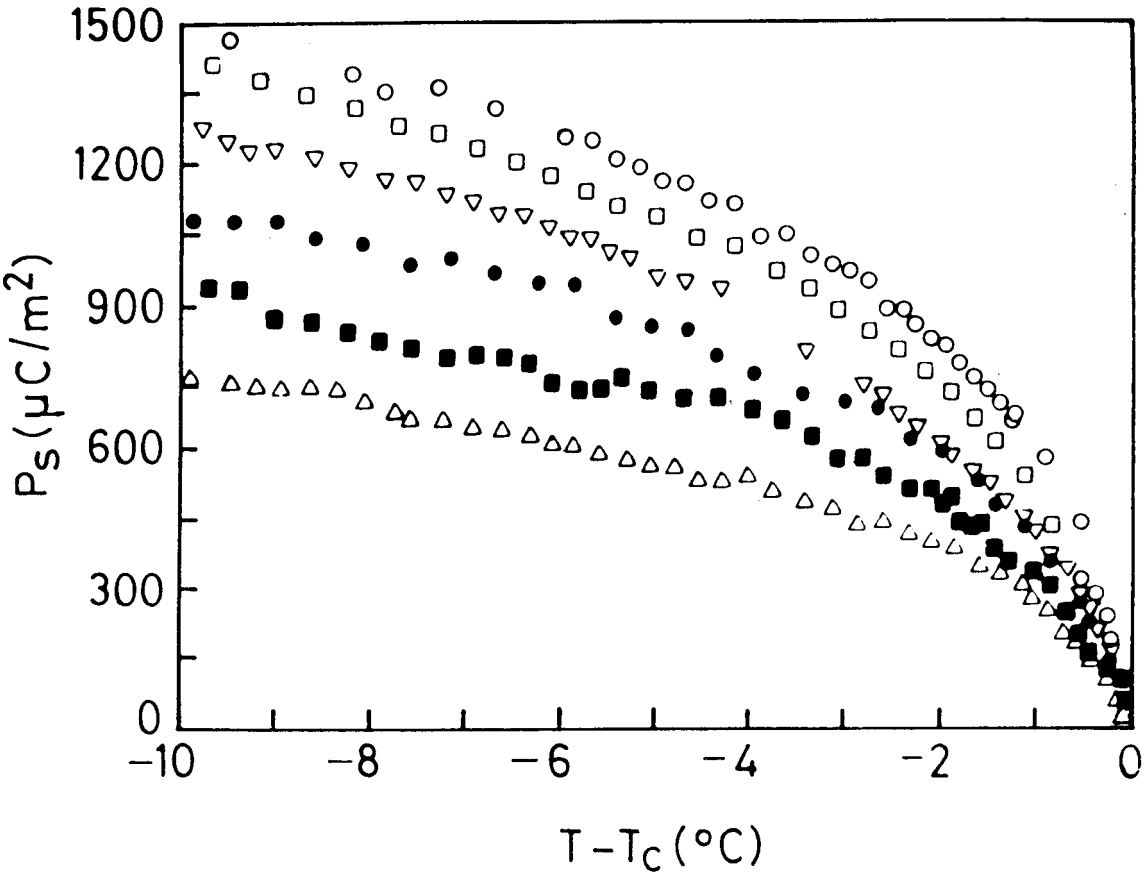

Fig.2.10. Thermal variation of spontaneous polarisation P_s for n = 7 (○), n = 8 (□), n = 9 (▽), n = 10 (●), n = 11 (■) and n = 12 (A) of series D.

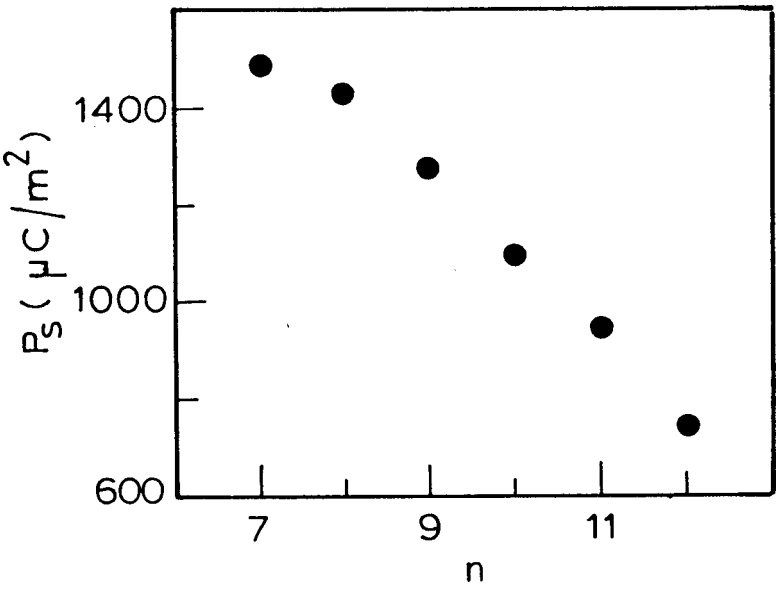

Fig.2.11. P_s at $T_c - T = 10°C$ as a function of chain length n.

2.4.2 Series B: Compounds with two chiral centres and with a CH_2 spacer group

Fig. 2.12 is a plot of P_s vs. T – T_c for the six liomologues of this group (n=7 to 12). The features observed are very similar to that of series D, viz., P_s decreases with increase in temperature and goes to zero continuously at T_c, the value of P_s decreases substantially as n increases (see Fig.2.13). However, tlie overall magnitude of P_s itself is much smaller for series B as compared to series D. For example, at $T - T_c = -10°C$ for 7th homologue it is 1500 $\mu C/m^2$ in series D and 650 $\mu C/m^2$ for series B (compare Figs. 2.11 and 2.13). As we see later, this appears to be due to the addition of a spacer group.

2.4.3 Series C: Compounds with one chiral centre without CH_2 spacer

The plots of P_s vs. $T - T_c$ for the six homologues (n = 7 to 12) of this series and tlie variation of P_s at $T - T_c = -10°C$ vs. chain length are given in Figs. 2.14 and 2.15. The behaviour observed is in agreement with those of series D and B. Results for this series show that reducing tlie number of asymmetric carbon atoms decreases the value of P_s. At $T - T_c = -10°C$, tlie 7th homologue of series C has P_s value 960 $\mu C/m^2$ as against P_s = 1500 $\mu C/m^2$ for series D. (A more detailed discussion of the effect of the second chiral atom is given later.)

2.4.4 Series A: Compounds with one chiral centre and a CH_2 spacer group

Plots of P_s versus temperature and P_s versus chain length arc given in Figs. 2.16 arid 2.17. The observed variations are in conformity with tlie behaviour of series D, B and C. The results on this series sliow the combined effect of reducing a chiral

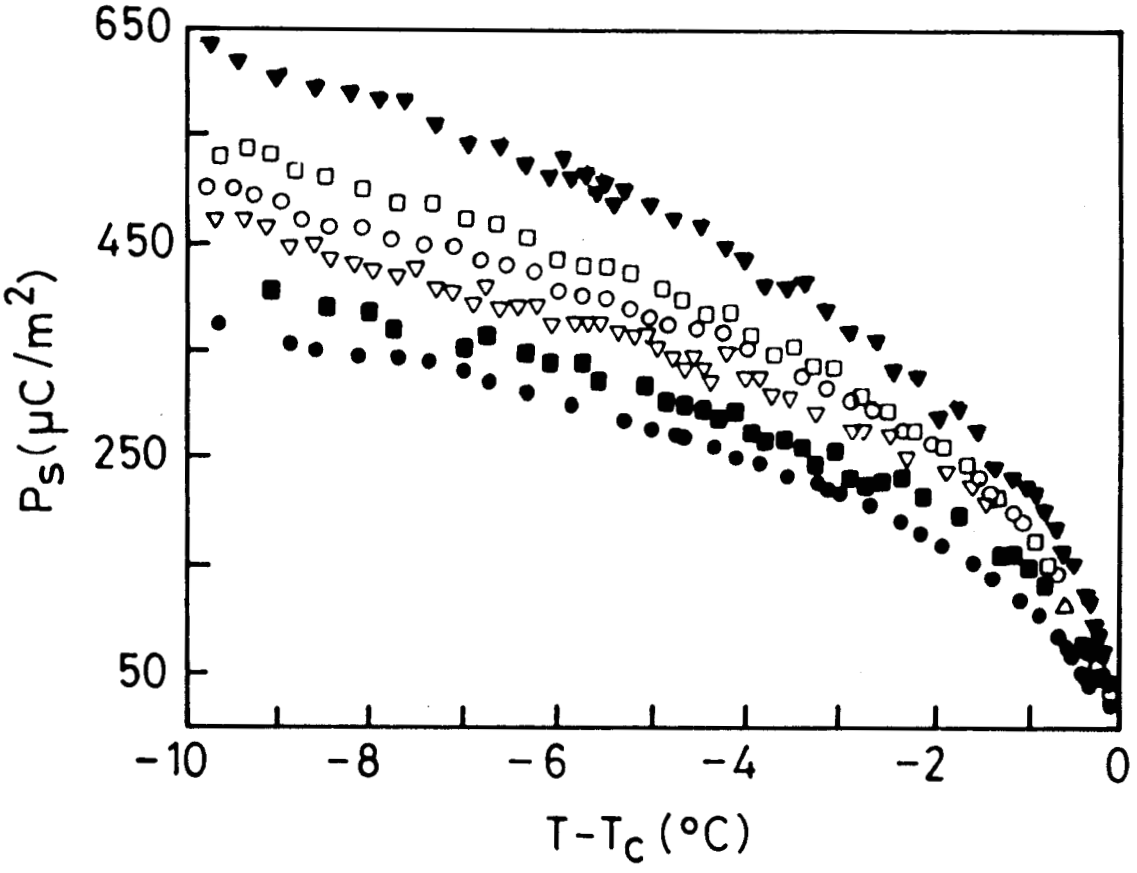

Fig.2.12. Thermal variation of spontaneous polarisation P_s for n = 7 (▼), **n** = 8 (□), n = 9 (○), n = 10 (▽), n = 11 (■) and n = 12 (●) of series B.

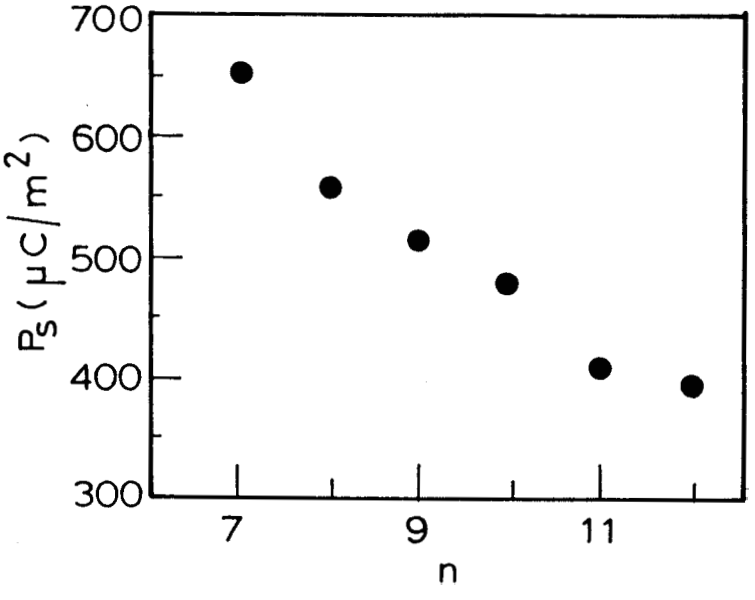

Fig.2.13. P_s at T_c – T = 10°C as a function of chain length n.

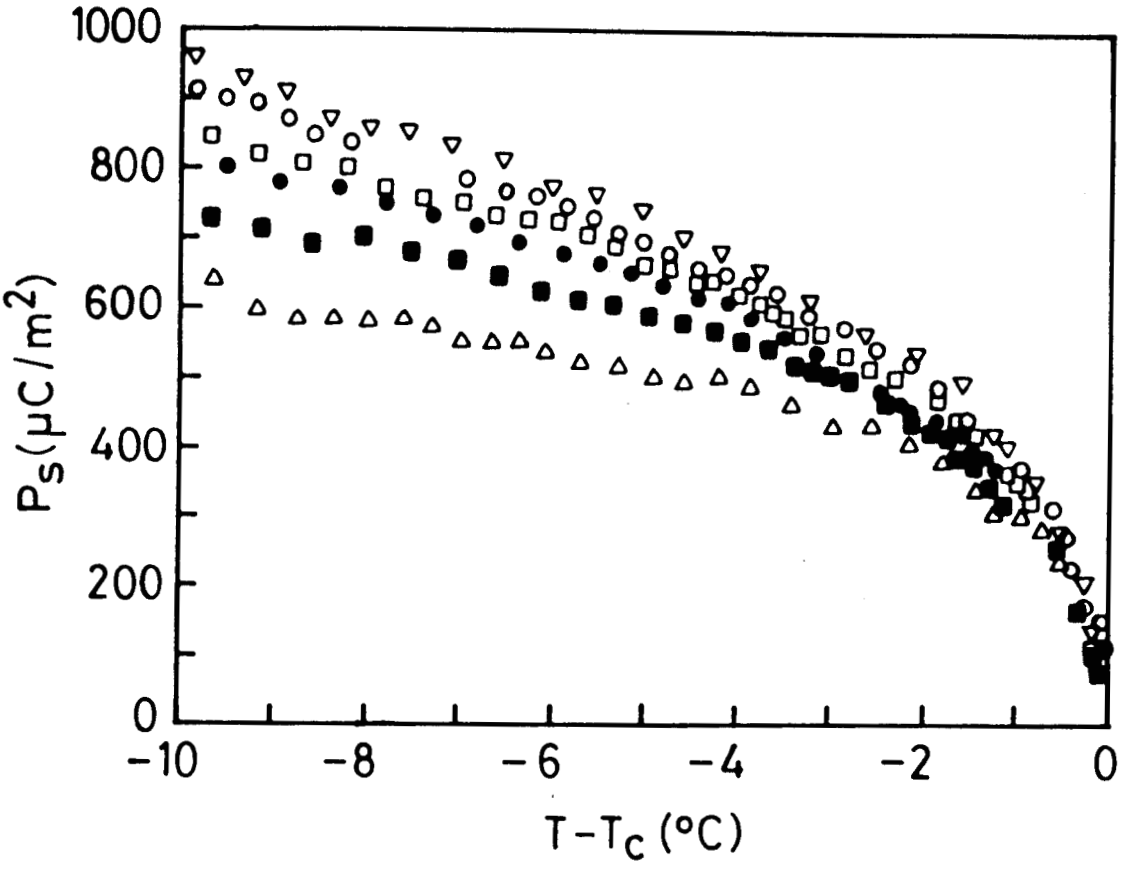

Fig.2.14. Thermal variation of spontaneous polarisation P_s for n = 7 (▽), n = 8 (○), n = 9 (□), n = 10 (●), n = 11 (■) and n = 12 (A) of series C.

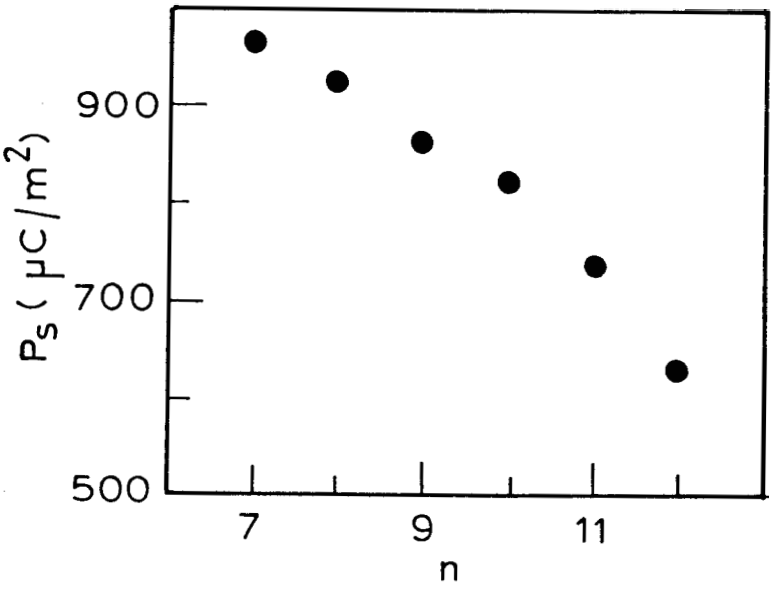

Fig.2.15. P_s at T_c – T = 10°C as a function of chain length n.

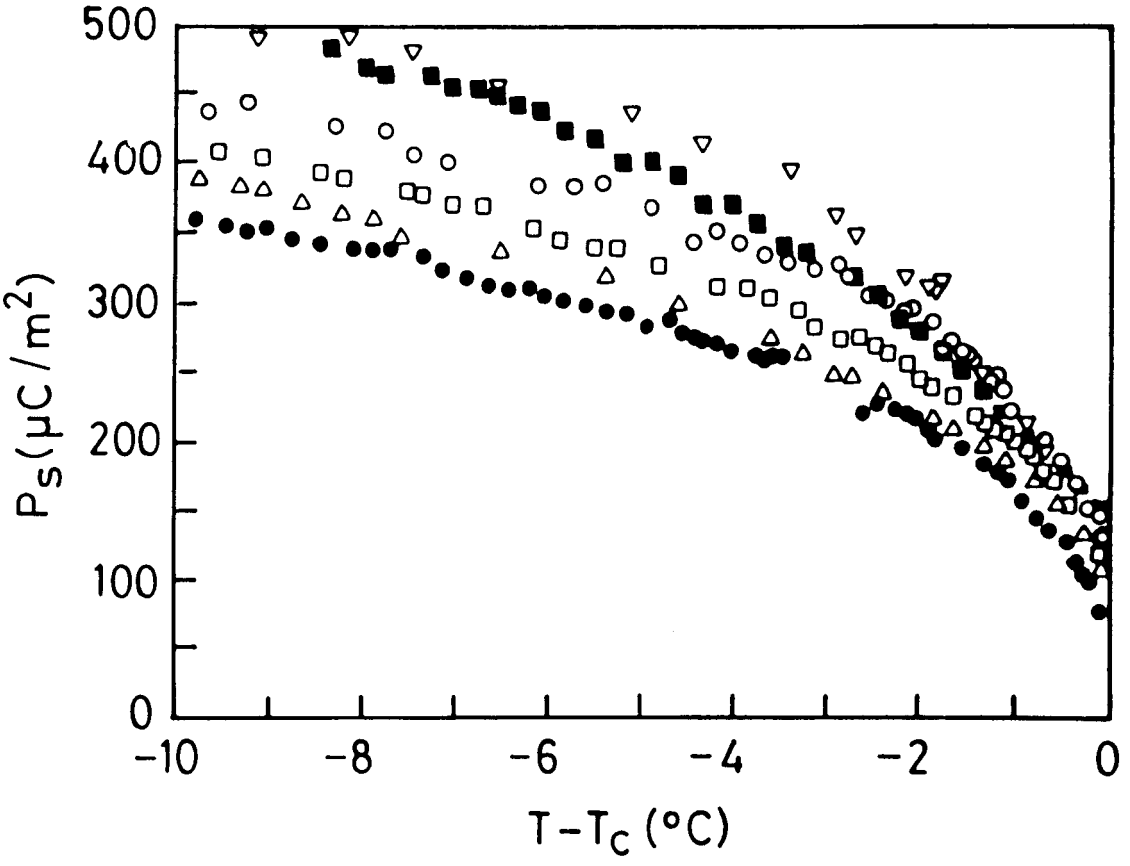

Fig.2.16. Thermal variation of spontaneous polarisation P_s for n = 7 (▽), n = 8 (■), n = 9 (○), n = 10 (□), n = 11 (A) and n = 12 (●) of series A

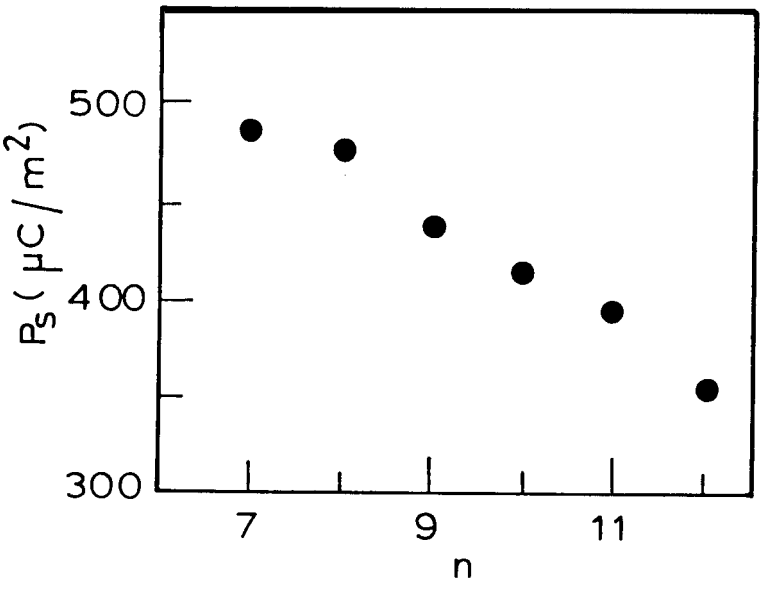

Fig.2.17. P_s at $T_c - T = 10°C$ as a function of chain length n.

atom and introducing a spacer group.

2.5 Discussion

In this section we analyse our results in terms of tlie effect of different parameters like, length of the alkyl chain, number of asymmetric carbon atoms and the role played by spacer groups, on the magnitude of P_s.

2.5.1 Effect of alkyl chain length

From Figs. 2.11, 2.13, 2.15 and 2.17 it is obvious that P_s is strongly dependent on the length of tlie alkyl chain. In all the four series of compounds studied, tlie P_s value is found to decrease with increasing chain length. This behaviour is in agreement with earlier observations (though an exception to this, viz., P_s increases with increasing chain length has also been reported earlier[15]). The decrease in P_s with increasing n can be accounted for by the "zig-zag" conformation of tlie molecules[37] (see Fig. 2.18). According to this model the value of P_s is controlled by the effective tilt angle θ_t of tlie tail portion of tlie molecule. As the effective tilt angle θ_t decreases with increasing n, P_s should also decrease as the chain length is increased.

2.5.2 Effect of the number of chiral groups and their locations

As seen from tables 2.1 to 2.4, the selected homologues series provide different mutual combinations of number and location of cliiral carbon atoms. The results obtained, described in tlie previous section, can be used to understand the effect of these subtle changes on the magnitude of P_s. The salient features which come out of such an analysis are mentioned below.

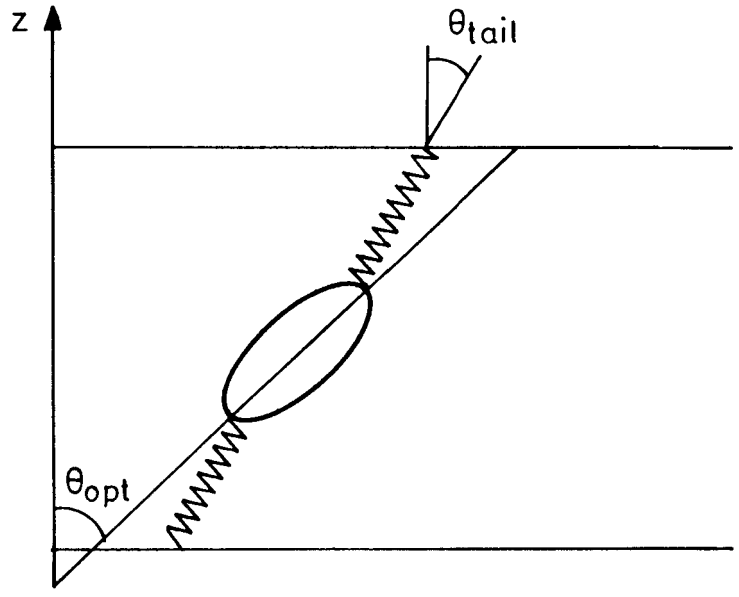

Fig.2.18. A zig-zag model for the molecular packing in the C* phase.

1. If a spacer group (CH_2 group in our case) is introduced between the core and the chiral carbon atoms, it would decrease the magnitude of P_s. This is found to be true for both single chiral group (series C arid A) and two chiral group(series D and B) structures. The decrease in the magnitude is substantial, being $\sim 50\%$. In fact such large changes occurririg due to the inclusion of a spacer group has been observed by Yoshino et *al.*,.[12] One possible explanation for this type of behaviour is that the presence of the spacer weakens tlie coupling between the dipole and the chiral centre enabling tlie dipole to rotate freely thus decreases the value of P_s.

2. It would appear that a simple way of increasing tlie magnitude of P_s is to increase the number of chiral carbon atoms. Although this is true, the relative increase is not very high. Only $\sim 30\%$ changes have been observecl between series D and C and series B and A. This may be compared to the role played by tlie spacer group mentioned above. This shows that although the enhancement of steric hindrance, got by tlie addition of a second chiral group, increases P_s, it may not be the only key factor. Thus it appears that to obtain higher P_s values it is better to position the chiral centre close to the core rather than having many chiral centres located away from tlie core.

In addition to the above two important factors which decide tlie magnitude of P_s, we have noticed that the presence of any bridging group between phenyl rings also plays a role. To see this let us compare the results for series D with those synthesised for example, by Bahr and Heppke[13] (MCPnOB series). (Note tliat the molecular structure of series D is very similar to that of MCPnOB series given in Fig. 2.19.) Structurally the two are identical except that in MCPnOB series the core is made of a biphenyl group (no bridging group) and in series D there is a polar bridging

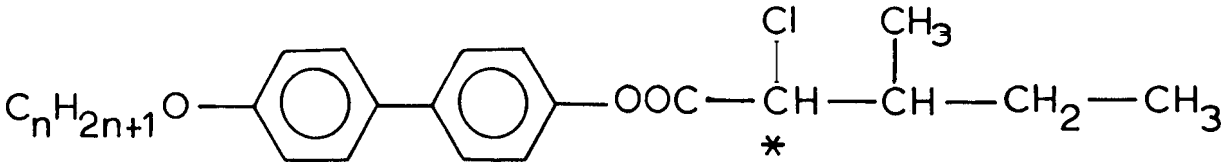

Fig.2.19. Molecular structure for MCPnOB Series.[13]

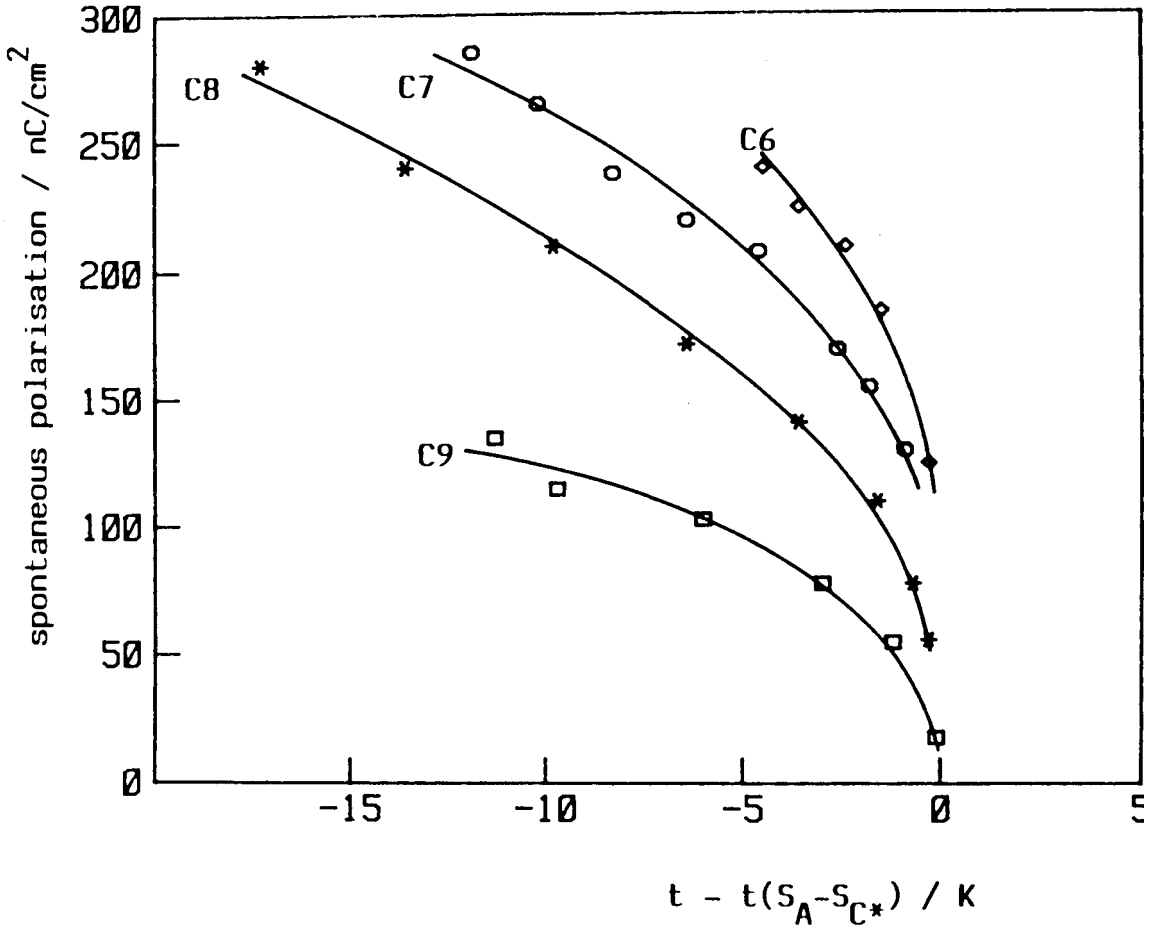

Fig.2.20. Temperature dependence of the spontaneous polarisation for the MCP-nOB Series.[13].

group CH=CHCOO between the phenyl rings. The P_s data of Balir arid Heppke for the MCPnOB series is reproduced in Fig. 2.20. Comparing this witli series D (Fig. 2.10), we see that -

1. The introduction of a bridging group between tlie two phenyl rings, albeit a polar one, has brought down tlie P_s by a factor of two, e.g., the saturation value of P_s of series D for n = 7 is $\approx 1500\mu C/m^2$ and for n = 7 of MCPnOB series it is about $3000\mu C/m^2$. The reason for which may be that -

   i The COO group in the core tilts one phenyl group with respect to the other thus providing an increased degree of freedom of rotation for the chiral part about the rest of the molecule.

   ii Though a polar group has been added, the increase in tlie length of the molecule due to tlie additional CH=CHCOO group has overcompensated tlie increase in the transverse dipole moment. As we see in our studies (Figs. 2.10, 2.12, 2.14 and 2.16) as well as in MCPnOB (Fig. 2.20) increasing the length of the molecule usually brings down P_s.

2. In series D as well as in MCPnOB both P_s and the rate of variation of P_s as a function of temperature, i.e., $\frac{dP_s}{dT}$ at T_c decrease as n increases. However in contrast to the MCPnOB series (and also the lactic acid derivatives[15]), the range of the SmA phase decreases with increasing chain length (see Fig. 2.1a-d). This is somewhat surprising for the following reasons. High resolution specific heat[20] and tilt angle [22] experiments have shown that one of the parameters controlling tlie nature of tlie A-C* transition is the temperature range of the A phase. In particular, it has been shown that tlie rate of variation of θ with temperature, $\frac{d\theta}{dT}$, increases with decreasing range of tlie A phase. Since

in the proximity of the transition, P_s can be taken to be linearly coupled to θ, $\frac{dP_s}{dT}$ should also behave tlic same, which is contrary to our experimental results.

2.5.3 Comparison of P_s data with the microscopic model

The thermodynamic model introduced by Pikin and Indenbom[38] and extensions of it proposed by the Ljubljana group[39,40] and independently by Huang et *al.*,[41] have been quite successful in explaining various experimental features of different physical properties of FLCs. But due to its phenomenological nature, the properties are not described in terms of microscopic parameters. With this in mind, Zeks et *al.*,[16,17] proposed a theory based on single particle potentials. Here we briefly describe this microscopic model and some of the consequences of it. We also attempt to arialyse the results obtained for series A,B,C and D in terms of the parameters of this model.

The theory is based on the assumption that the transverse molecular ordering is induced by the tilt of the molecules only and not due to the interaction between the dipoles of tlie molecules (experimental results substantiate such an assumption). The tilt biases the free rotations of the molecules about their long axis and induces ordering of tlie dipoles perpendicular to this axis. The degree of dipolar ordering depends on the angle of orientation ψ of the dipole in a plane perpendicular to the long molecular axis. The coordinates are chosen such that when $\psi = 0$ the dipole μ is perpendicular to the plane of the tilt and parallel to the direction of P,. A single particle potential V (ψ) for the rotation of the molecule around its long axis can he expressed as

$$V(\psi) = -a_1\theta cos\psi - a_2\theta^2 cos2\psi \qquad (2.2)$$

Here the first term is linear in θ and exists only for chiral molecules ancl is analogous to the bilinear coupling term (see Chapter III) in the phenomenological model. When the coefficient a_1 is positive the tilt tends to align the transverse dipoles in the direction $\psi = 0$ and for perfect order tlie first term would be equal to -$a_1\theta$. The second term is quadratic in θ arid is not of chiral character and exists in all tilted systems, chiral or achiral. If $a_2 \neq 0$, this leads to a quadrupolar ordering in the direction perpendicular to the tilt and is analogous to the biquadratic coupling in the phenomenological model. The expected relation between the magnitudes of the two parts of the potential is $a_1\theta \ll a_2\theta^2$ except close to the transition, where θ is very small. Again this is true of bilinear and biquadratic terms. The thermal average of $cos\psi$ at any temperature T^oK is given by,

$$< cos\psi > \; = \; \frac{\sum_o^{2\pi} cos\psi exp(-V/kT)d\psi}{\sum_o^{2\pi} exp(-V/kT)d\psi} \tag{2.3}$$

ancl can he used to calculate the value of P_s,

$$P_s = \rho\mu < cos\psi > \tag{2.4}$$

where ρ is the particle density and μ tlie transverse dipole moment of tlie molecule. Using eqn. 2.3 and substituting for V, it has been shown that[42] P_s can be written as

$$P_s = \rho\,\mu\,\theta\,a_1\,\frac{2kT + a_2\theta^2}{4(kT)^2 + (a_1\theta)^2 + (a_2\theta^2)^2} \tag{2.5}$$

From eqn. 2.5 it is clear that knowing the temperature dependence of P_s and θ tlie coefficients a_1 and a_2 can be evaluated. In order to see the effect of molecular structure on the values of a_1 and a_2 we have calculated these parameters for a representative homologue (n=10) of each series. As, such

a calculation needs the tilt angle data, we have measured 0 by the X-ray diffraction method, described earlier. Figures 2.21 to 2.24 are the plots of 0 vs. $(T_c - T)$ for the four compounds. It is seen from these figures that the tilt angle is almost same for all the four series suggesting that small structural changes rnay not alter the value of 0. Since tlie fitting to eqn. 2.5 needs θ arid P_s at the same temperature and experimentally it was not feasible to achieve this, we made use of a functional description of tlie 0-data. It may be recalled here that extensive studies on the SmA-SmC* transition have shown that the tilt angle in tlie C* phase can be described by tlie expression given by an extended mean field model[43]

$$\theta = R\left[\left(1 - \frac{3t}{t_o}\right)^{1/2} - 1\right]^{1/2} \tag{2.6}$$

where t = $\frac{T - T_c}{T_c}$, R and t_o are parameters cliaracterising the transition. Figs.2.21-2.24 also show the fit of the data to eqn. 2.6. The fitting is very good and therefore eqn. 2.6 can be used to calculate values of θ in eqn. 2.5.

Neglecting tlie θ^4 term, we can rewrite eqn. 2.5 as

$$P_s = A_1\theta\frac{A_2T + A_2A_3\theta^2}{T^2 + A_2^2\theta^2} \tag{2.7}$$

where

$$A_1 = \rho\mu, \quad A_2 = \frac{a_1}{2K} \quad and \quad A_3 = \frac{a_2}{2K} \tag{2.8}$$

We have fitted our P_s data to eqn. 2.7 using a lion-linear least square fit program based on the marquardt algorithm by floating the parameters A_1, A_2 and A_3 for tlie four compounds. Figures 2.25-2.28 are tlie plots of P_s vs. $(T_c - T)$ for the four compounds. The solid lines are tlie fit to equation 2.7 and show that tlie fitting is quite good. The values of A_1, A_2 and A_3 for tlie four compounds arc given in table 2.6.

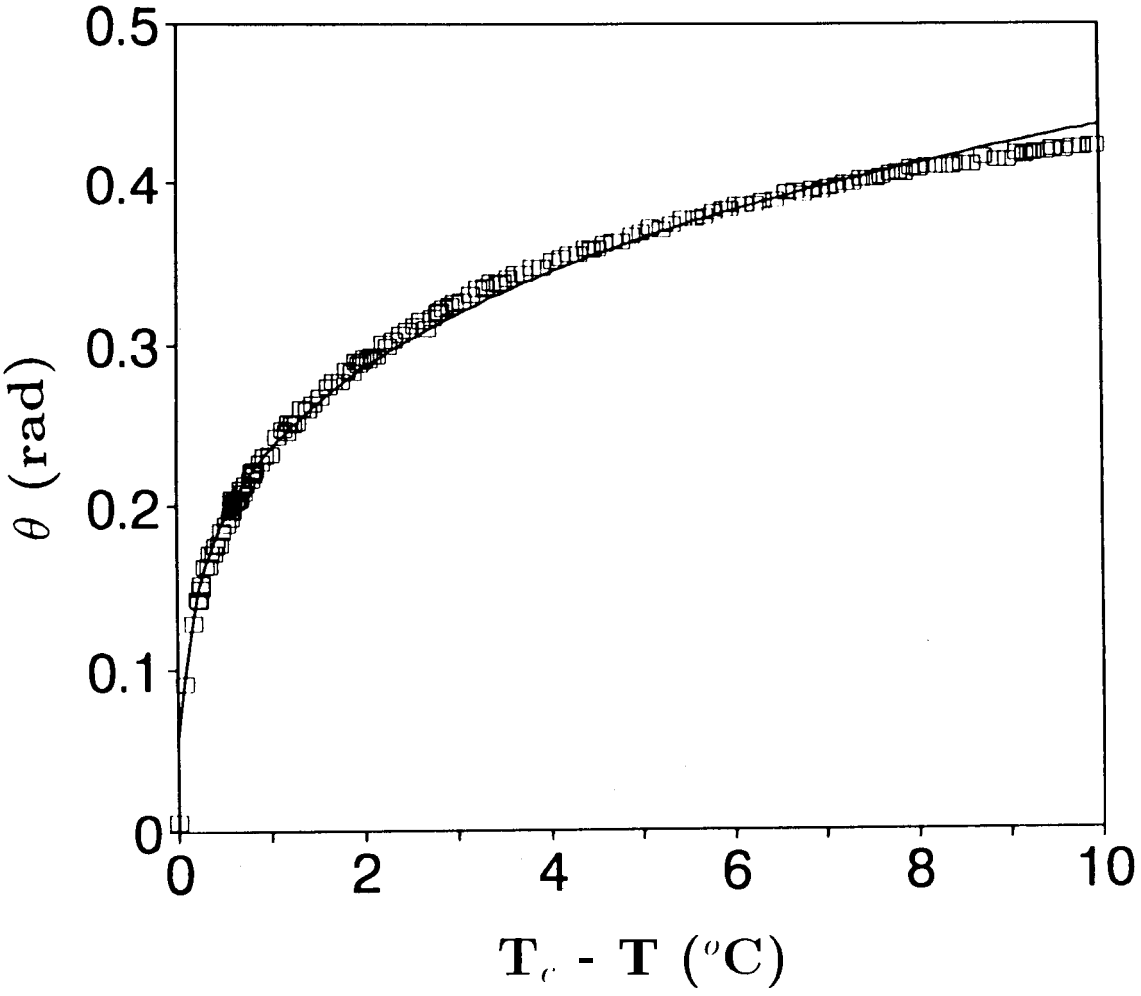

Fig.2.21. Thermal variation of tilt angle θ for A_{10}; squares represent experimental data and the line fit to eyn. (2.6).

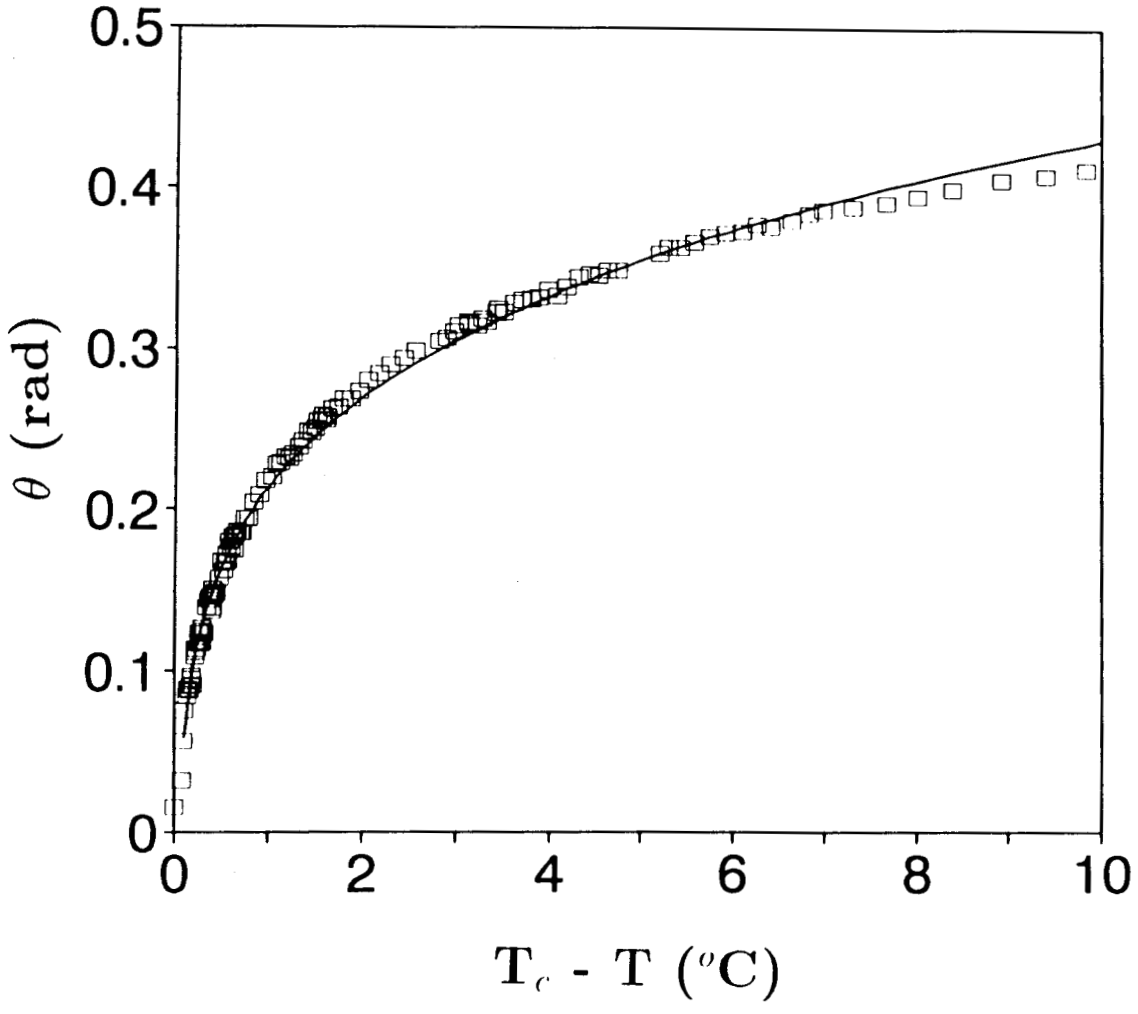

Fig.2.22. Thermal variation of tilt angle θ for B_{10}; squares represent experimental data and the line fit to eqn. (2.6).

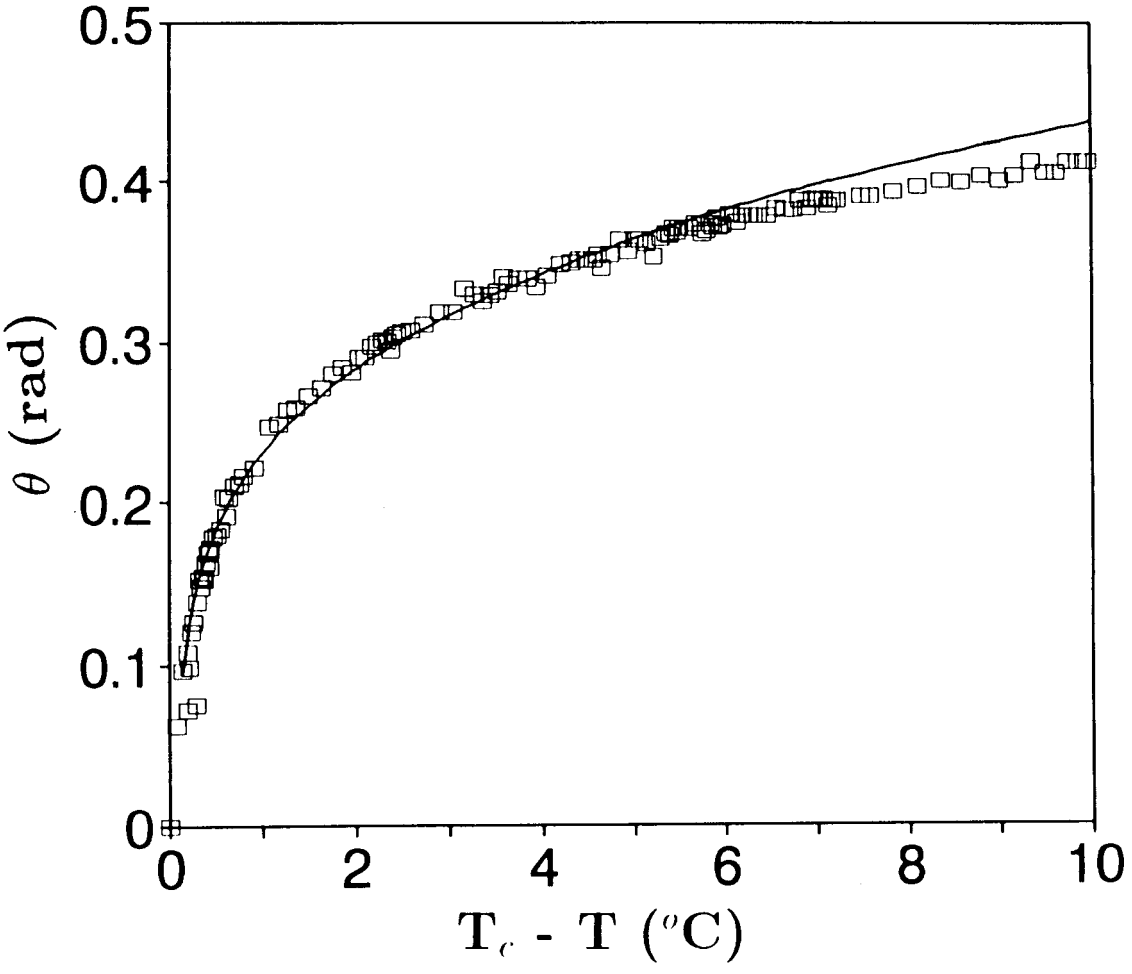

Fig.2.23. Thermal variation of tilt angle 6 for C_{10}; squares represent experimental data and the line fit to eqn. (2.6).

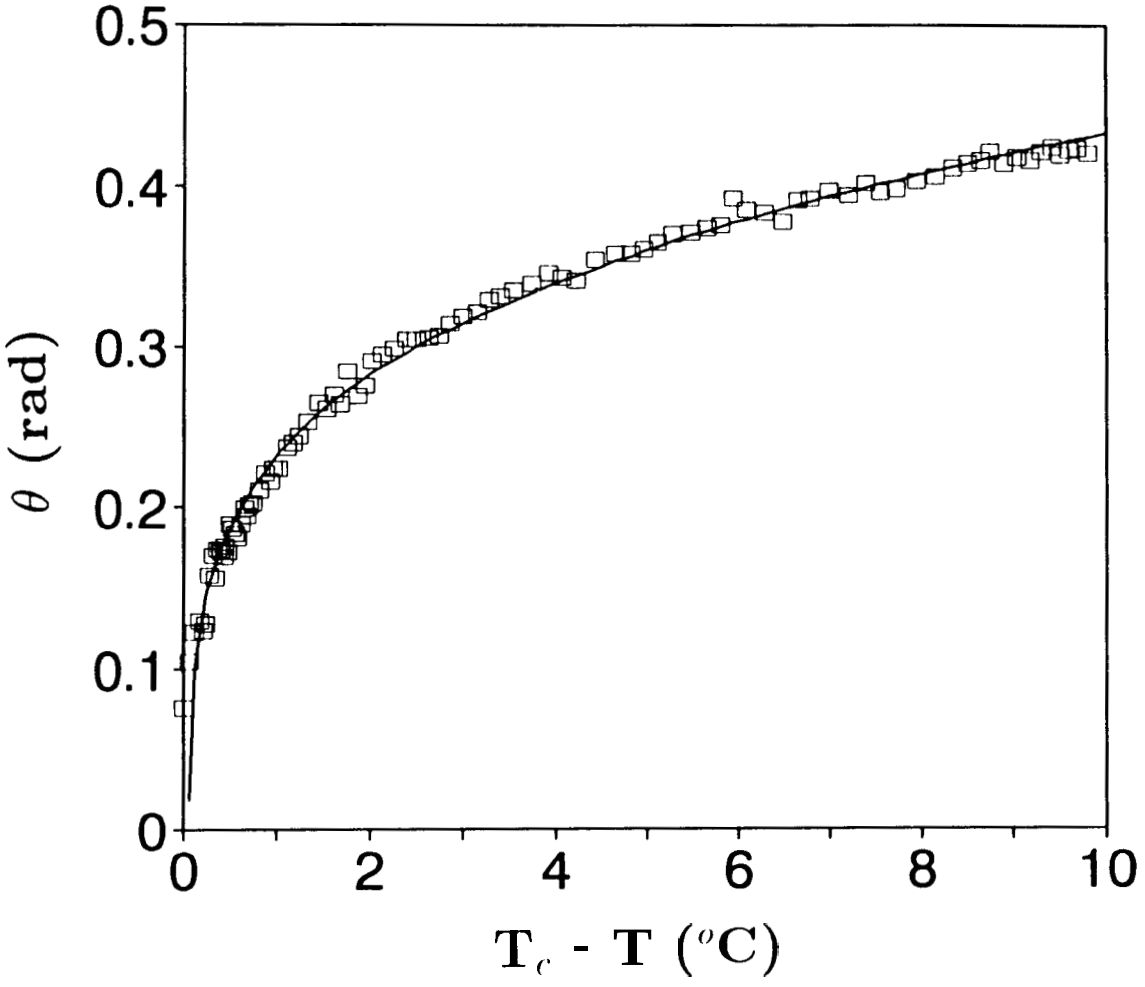

Fig.2.24. Thermal variation of tilt angle θ for D_{10}; squares represent experimental data and the line fit to eqn. (2.6).

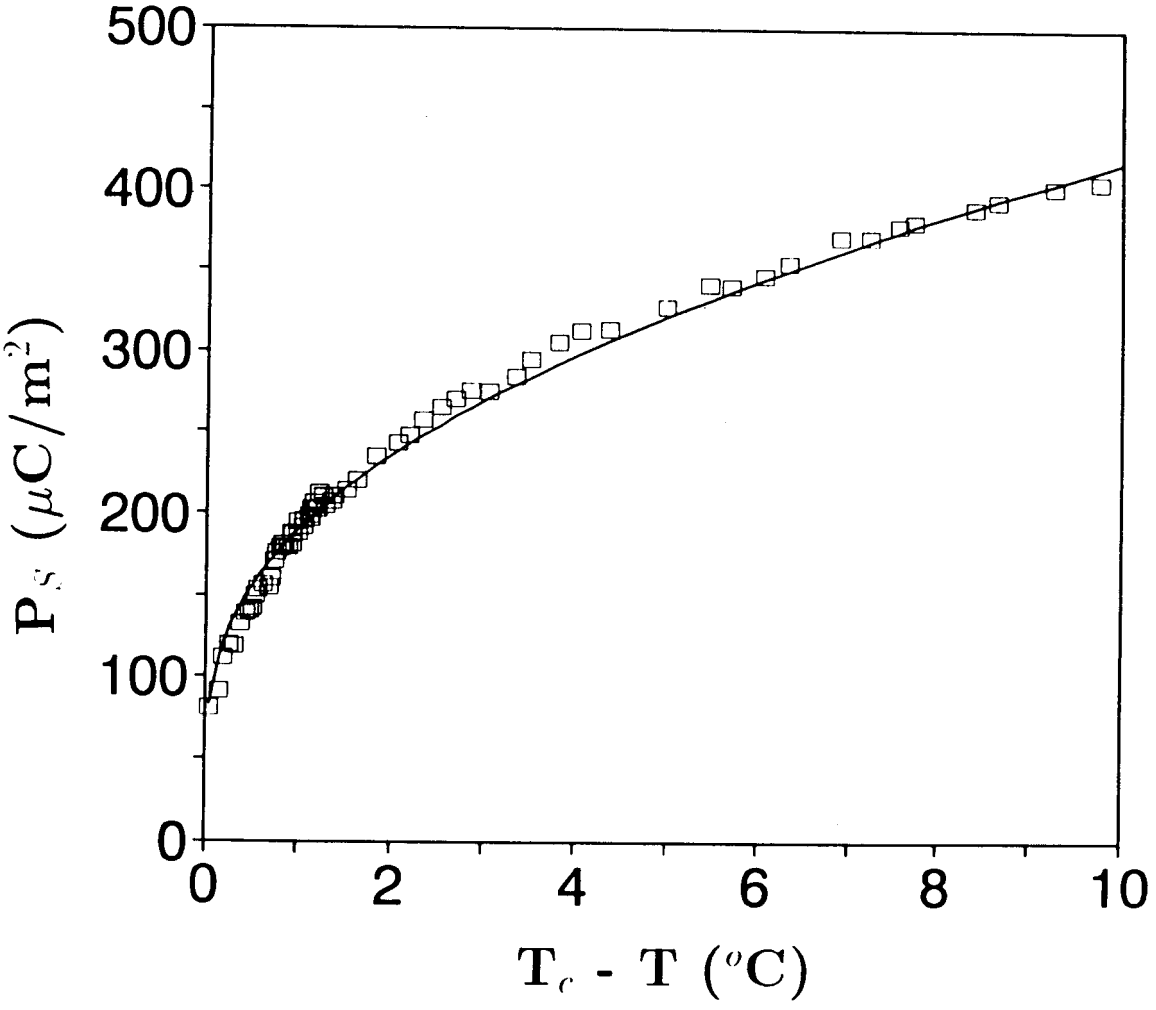

Fig.2.25. Fit of the P_s data to eq. (2.7) given by the microscopic model for A_{10}; squares represent data and the line the fit.

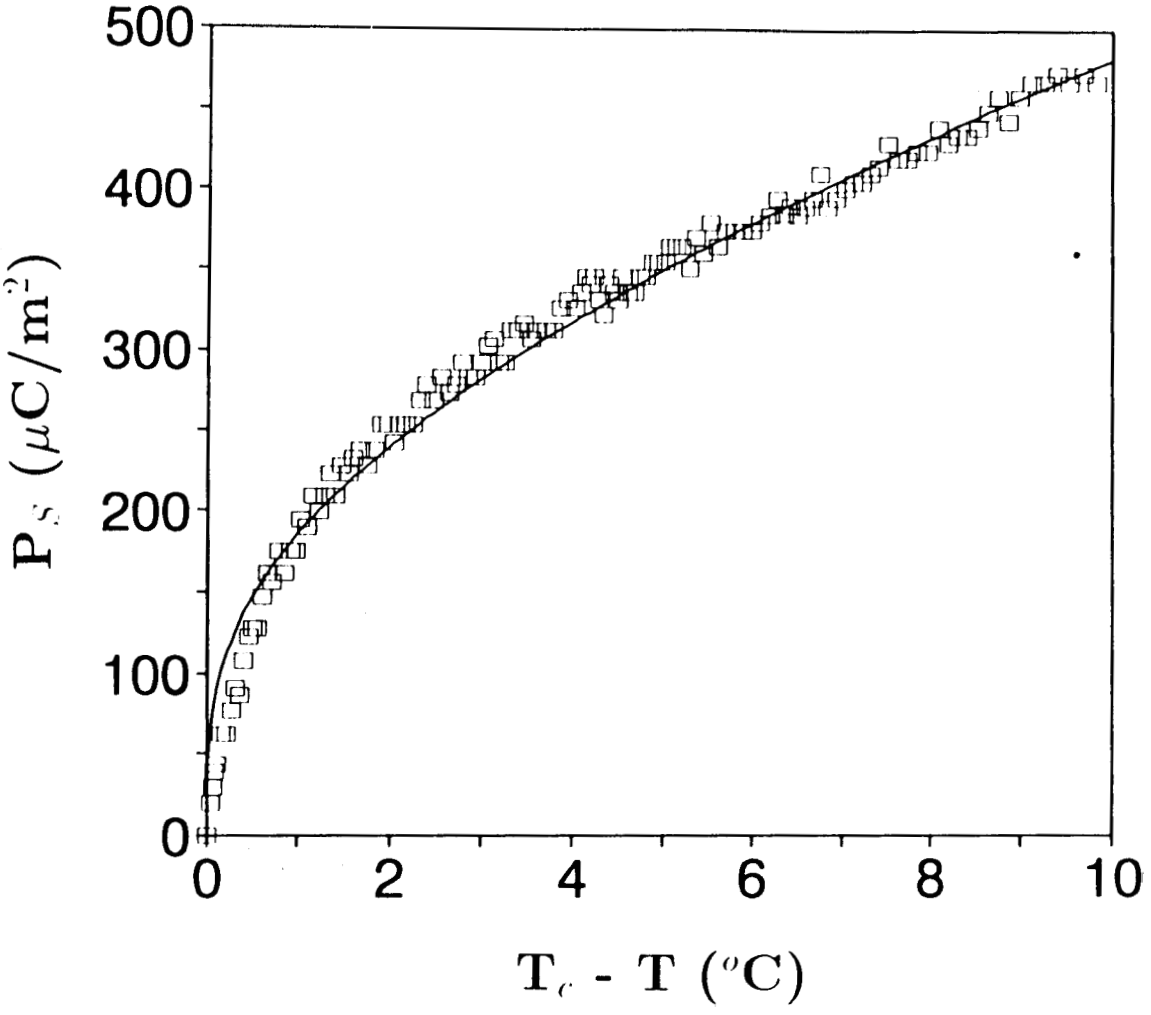

Fig.2.26. Fit of the P_s data to eq. (2.7) given by the microscopic model for B_{10}; squares represent data and the line the fit.

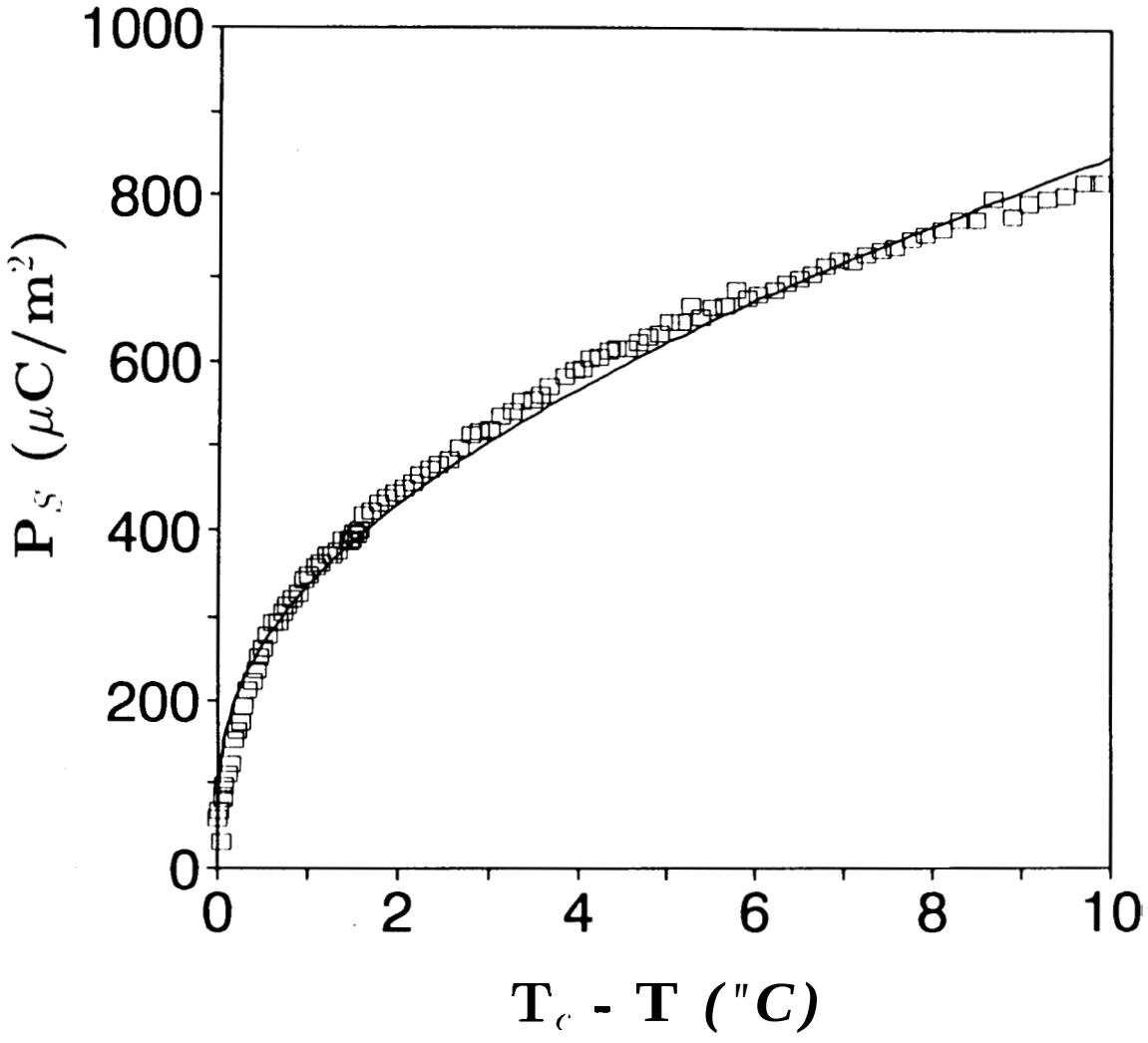

Fig.2.27. Fit of tlie P_s data to eq. (2.7) given by the microscopic model for C_{10}; squares represent data and the line the fit.

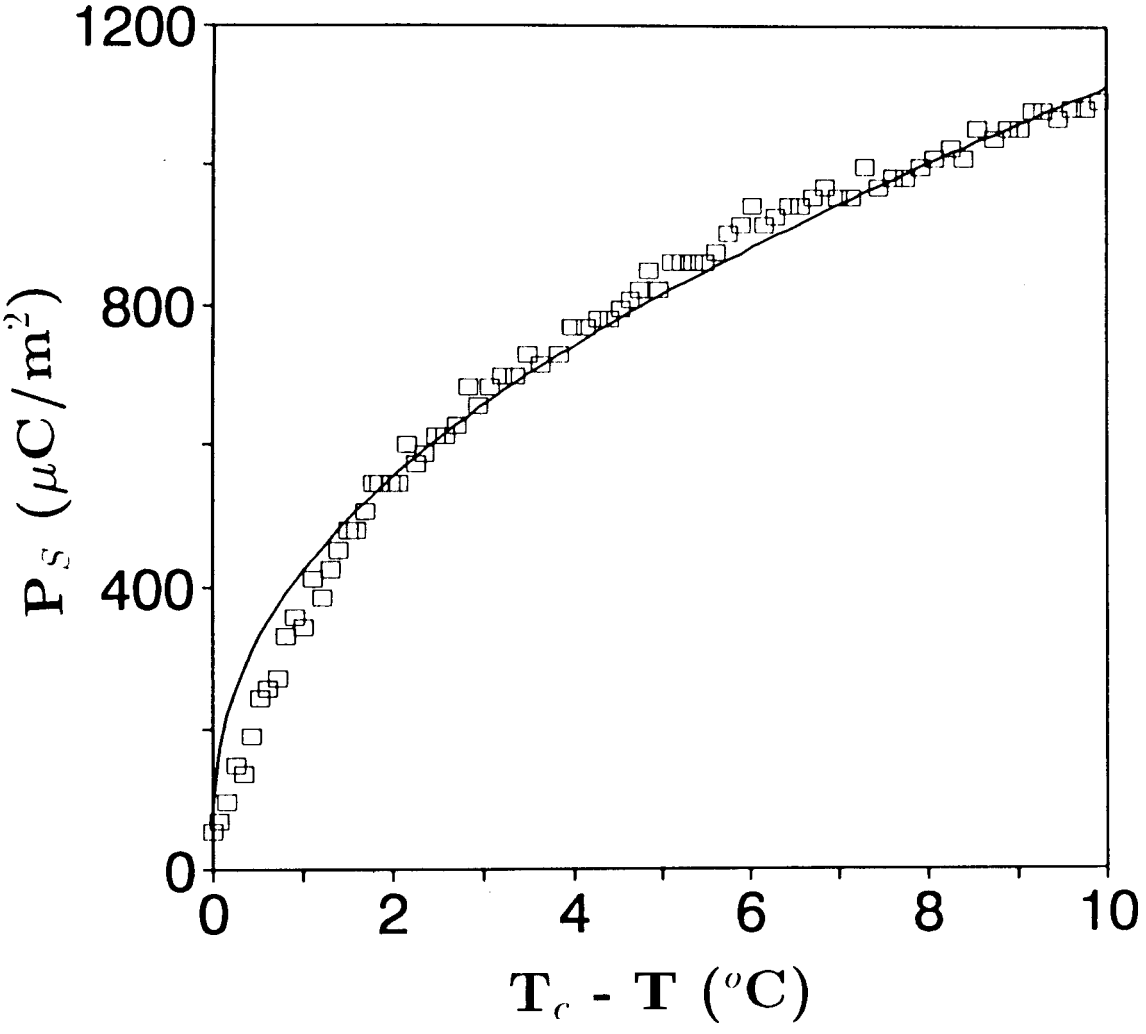

Fig.2.28. Fit of the P_s data to eq. (2.7) given by the microscopic model for D_{10}; squares represent data and the line the fit.

Table 2.6

Values of coefficients obtained from fit to microscopic model

Compound	A_1 ($\mu C/m^2$)	A_2 (J/k)	A_3 (J/k)	a_1 (J)	a_2 (J)	$\tilde{C} = a_1/A_1$ (Vm^2)	a_1/a_2
A 10	263	217.79	842.88	6.01E-21	2.33E-20	2.29E-17	0.258
B 10	258	216.65	955.57	5.98E-21	2.64E-20	2.31E-17	0.226
C 10	315	277.10	2462.5	7.65E-21	6.8E-20	2.43E-17	0.112
D 10	326	321.95	3125.52	8.89E-21	8.63E-20	2.73E-17	0.103

It is known[44] that close to the transition, the dominant coupling term between P_s and θ is the bilinear coupling coefficient C, which can be taken as a measure of P_s for any given compound, although away from tlie transition, the biquadratic contribution is quite large. In terms of the parameters obtained from eqn. 2.7, the coefficient C can be written as[16]

$$C = \frac{a_1}{\mu}$$

Using eqn.2.8

$$C = \frac{a_1}{\mu} = \frac{a_1}{A_1/\rho} = \frac{\rho a_1}{A_1} \tag{2.9}$$

Since ρ, the number density is riot expected to vary drastically between the different series (A,B,C and D) of compounds, it can he treated as a constant and one can write,

$$\tilde{C} = \frac{C}{\rho} = a_1/A_1 \tag{2.10}$$

Table 2.6 also gives the values of $\tilde{C}$ calculated for the 10th homologue of series A,B,C and D. It is observed that $\tilde{C}$ is lowest for series A and highest for series D. More explicitly $\tilde{C}$ for series A < series B < series C < series D. Quite interestingly, this is the way the P_s also varies between different series.

According to the theory,[16,17] close to the transition, the dipolar term dominates the potential while away from it the quadrupolar term takes over. This behaviour is in fact seen in the experimental data also. Listecl in table 2.6 are the ratios of quadrupolar to dipolar terms (= $\frac{a_2\theta}{a_1}$) for the 10th homologues of the four series. Such a feature has been observed by Buka et *al.*,[42] also.

References

[1] R.B.Meyer, L.Liebert, L.Strzelecki and P.Keller, J. *de Phys.* Lett., 36, 69 (1975).

[2] N.A.Clark and S.T.Lagerwall, *Appl. Phys.* Lett., 36, 899 (1980).

[3] N.A.Clark, M.A.Handschy and S.T.Lagerwall, *Mol. Cryst.* Liquid *Cryst.*, 94, 213 (1983).

[4] S.T.Lagerwall, B.Otterholm and K.Skarp, *Mol. Cryst.* Liquid *Cryst.*, 152, 503 (1987).

[5] L.S.Beresnev, L.M.Blinov, M.A.Osipov and S.A.Pikin, *hlol. Cryst. Liquid Cryst.*, **158A**, 1 (1988).

[6] J.W.Goodby, E.Chin, T.M.Leslie, J.M.Geary and J.S.Patel, *J. Am. Chem. Soc.*, **108**, 4729 (1986).

[7] D.M.Walba, S.C.Slater, W.M.Thurmes, N.A.Clark, M.A.Handschy, F.Supon, *J. Am. Chem. Soc.*, **108**, 5210 (1986).

[8] K.Mohr, S.Kohler, K.Worm, G.Pelzl, S.Diele, H.Zaschke, D.Demus, G.Anderson, I.Dahl, S.T.Lagerwall, K.Skarp and B.Stabler, *Mol. Cryst. Liquid Cryst.*, 146, 151 (1987).

[9] R.B.Meyer, *Mol. Cryst.* Liquid *Cryst.*, 40, 33 (1977), and P.Keller, L. Liebert and S.Strzelecki, J. *de Phys.*, 37, 3 (1976).

[10] M.Luzar, V.Rutar, J.Seliger and R.Blinc, *Ferroelectrics*, **58**, 115 (1984).

[11] J.S.Patel and J.W.Goodby, *Mol. Cryst. Liquid Cryst.*, 144, 117 (1987).

[12] K.Yoshino, M.Ozaki, T.Sakurai, K.Sakamoto and M.Honma, *Japan* J. *Appl. Phys.*, 23, 1,175 (1984).

[13] Ch. Bahr and G.Heppke, *Mol. Cryst. Liquid Cryst.* Lett., **4,** 31 (1986); *hfol. Cryst. Liquid Cryst.*, 148, 29 (1987).

[14] T.Uemoto, K.Yoshino and Inuishi, *Japan J. Appl. Phys.*, **18,** 126 (1979).

[15] B.Otterholm, C.Alstermark, K.Flatischler, A.Dahlgren, S.T.Lagerwall and K.Skarp, *Mol. Cryst. Liquid Cryst.*, 146, 189 (1987).

[16] B.Zeks, T.Carlsson, C.Filipic and B.Urbanc, *Ferroelectrics*, 84, 3 (1988).

[17] B.Urbanc and B.Zeks, Liquid *Crystals*, 5, 1075 (1989).

[18] B.Shivkumar, B.K.Sadashiva, S.Krishna Prasad and S.M.Khened, *Ferroelectrics*, 114, 273 (1991).

[19] J.W.Goodby and E.Chin, *J. Am. Chem. Soc.*, 108, 4736 (1986).

[20] C.C.Huang and S.C.Lien, *Phys. Rev.,* A31, 2621 (1985).

[21] S.C.Lien and C.C.Huang, *Phys. Rev.*, A30, 624 (1984).

[22] S.Krishna Prasad, V.N.Raja, D.S.Shankar Rao, G.G.Nair and M.E.Neubert, *Phys.* Rev., A42, 2479 (1990).

[23] K.H.Yang, J. *Appl. Phys.*, 64, 4780(1988).

[24] J.S.Patel, T.M.Leslie and J.W.Goodby, *Ferroelectrics*, 59, 137 (1984).

[25] B.I.Ostrovskii, A.Z.Rabinovich, A.S.Sonin, A.Strukov and N.I.Chernova, J.E.*T.P.* Lett., 25, 70 (1977).

[26] L.J.Yu, H. Lee, C.S.Bak and M.M.Labes, *Phys. Rev. Lett.*, 36, 388 (1976).

[27] S.S.Bawa, A.M.Biradar, K.Saxena and Subhas Chandra, Rev. *Sci. Instrum.*, 59, 2023 (1988).

[28] P.Pieranski, E.Guyon and P.Keller, *J. de Phys.*, 36, 1005 (1975).

[29] C.Rosenblatt, R.Pindak, N.A.Clark and R.B.Meyer, Phys. *Rev.* Lett., **12,** 1220 (1979).

[30] K.Skarp, I.Dahl, S.T.Lagerwall and B.Stebler, *Mol. Cryst.* **Liquid** *Cryst.*, 114, 283 (1984).

[31] K.Miyasato, S.Abe, H.Takezoe, A.Fukuda and E.Kuze, *Japan* J. *Appl.* Phys., 22, L661 (1983).

[32] H.Diamant, K.Drenck and R.Pepinsky, Rev. Sci. *Instrum.*, 28, 30 (1957).

[33] C.B.Sawyer and C.H.Tower, *Phys.* Ilev., 35, 269 (1930).

[34] See for example, F.Jona and G.Shirane, Ferroelectric Crystals (Pergamon Press, New York, 1962).

[35] G.Spruce and R.D.Pringle, Liquid Crystals, 3, 507 (1988).

[36] S.Krishna Prasad, R.Shashidhar, B.R.Ratna, B.K.Sadashiva, G.Heppke and S.Pfeiffer, Liquid Crystals, 2, 111 (1987); S.Somasekhar, *Ph. D. The*sis, University of Mysore (1988).

[37] R.Bartolino, J.Doucet and G.Durand, *Ann. Phys.*, 33, 389 (1978).

[38] S.A.Pikin and V.L.Indenbom, Sou.*Phys.Usp.*,**21**, 487(1978).

[39] T.Carlsson, B.Zeks, A.Levstik, C.Filipic, I.Levstik and R.Blinc, *Phys.Rev.***A36**, 1484(1986).

[40] T.Carlsson, B.Zeks, A.Levstik and R.Blinc, hlol. *Cryst.* Liquid *Cryst.*, 163, 11(1988).

[41] S.Dumrangrattana and C.C.Huang, *Phys.*Rev.*Lett.*,**56**, 464(1986).

[42] A.Buka, K.Siemensmeyer and H.Stegemeyer, *Liquid Crystals*, **6**, 701(1989).

[43] C.C.Huang and J.M.Viner, *Phys. Rev.*, A25, 3385(1982).

[44] S.Krishna Prasad and Geetha G.Nair, *Mol. Cryst. Liquid Cryst.*, *202*, 91(1991).